

SWIFT-UVOT-CALDB-21-R00

Date Original Submitted: *January 1, 2012*

Prepared by: *Paul Kuin*

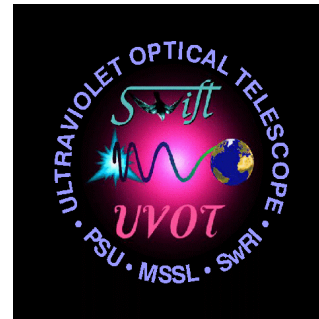
Date Revised:

Revision #0

Revised by: *Paul Kuin*

Pages Changed: *all*

Comments:



The wavelength calibration of the Swift UVOT Grisms

1 Summary

This product provides the in-orbit anchor point and dispersion of the first and second order grism spectra. This document describes the determination of, and the accuracy of the *Swift* UVOT uv and V grism wavelength calibration as based on the adjusted Zemax optical model and applies to both the nominal and clocked modes.

Table of contents

1 SUMMARY.....	1
TABLE OF CONTENTS	2
2 SCOPE.....	3
3 CHANGES:.....	3
4 REASON FOR UPDATE:	3
5 EXPECTED UPDATES:.....	3
6 CAVEAT EMPTOR:.....	3
DATA USED.....	4
7 DESCRIPTION OF ANALYSIS: INTRODUCTION.....	5
7.1 The anchor point	6
7.1.1 New method with the anchor point in the first order.....	6
7.1.2 The ‘old’ method with anchor point in the zeroth order	7
7.1.3 Finding the anchor point for the second order.....	8
7.2 Dispersion.....	8
7.2.1 dispersion with the anchor in the zeroth order	8
7.2.2 dispersion with the anchor in the first order (new method).....	9
8 THE PRELIMINARIES TO THE WAVELENGTH CALIBRATION	10
8.1 Use of the Zemax UVOT optical model.....	10
8.2 Determination of the boresight position for the grism image in first order	10
8.3 Determination of the scale factor for the model in the dispersion dimension	11
8.4 The anchor point position in the calibration image	13
8.5 No Anchor point adjustment to account for the boresight point drift.	14
8.6 Fitting to ground calibration data [nominal UV grism mode only]	14
9 THE WAVELENGTH FIT OF SPECTRA ACROSS THE DETECTOR.....	15
10 ERROR ANALYSIS OF THE NEW CALIBRATION.....	16
10.1 UV Nominal Grism.....	16
10.1.1 Accuracy of the anchor point for the UV nominal grism calibration.....	19
10.1.2 Accuracy of the wavelengths using the uv nominal grism calibration file	20
10.2 UV clocked grism	28
10.2.1 Accuracy of the anchor point for the uv clocked grism calibration	30
10.2.2 Accuracy of the wavelengths using the uv clocked grism calibration file	31
10.3 V nominal grism	36
10.3.1 Accuracy of the anchor point for the V nominal grism calibration	38
10.3.2 Accuracy of the wavelengths using the V nominal grism calibration file	38
10.4 V clocked grism	42

10.4.1 Accuracy of the anchor point for the V clocked grism calibration	43
10.4.2 Accuracy of the wavelengths using the V clocked grism calibration file	43
11 DISCUSSION AND SUMMARY.....	47
12 REFERENCES.....	49
13 LARGER TABLES.....	49

2 Scope

This document contains a description of the calibration analysis performed to produce a solution for the anchor point and dispersion of the wavelengths in the first and second order grism spectra for the UVOT calibration database (CALDB). The information that is provided includes a description of the wavelength calibration method, the accuracy of the new calibration and some pre-launch ground calibration results.

3 Changes:

An initial wavelength calibration was released on 4 May 2006, but without full CALDB documentation. This document will describe the 4 May 2006 release briefly, but mainly describes the new release.

4 Reason For Update:

N/A

5 Expected Updates:

N/A

6 Caveat Emptor:

The solution of the dispersion was optimised for the blue end of the spectrum. The second order calibration has only been partially completed.

Data used

Observational data was used to obtain the in-orbit wavelength calibration, as well as model data from the Zemax^{*} optical model for the grism. The most recent wavelength calibration used the emission lines in Wolf-Rayet stars of the listed spectral types since their width is similar to the resolution, yet they are strong. The spectra of the WR52 and WR86 illustrate this clearly; they were used for much of the UV grism wavelength calibration.

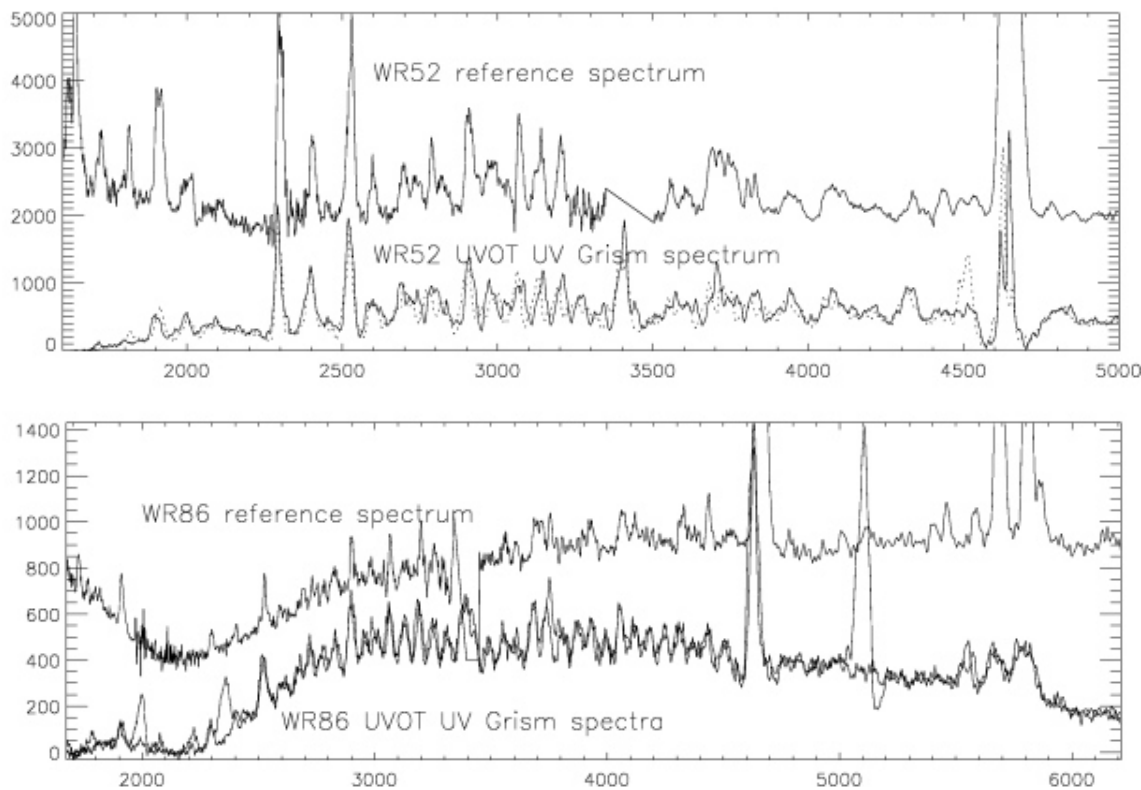


Figure 1: Using the strong emission line spectra of WR stars for the calibration. For two of the wavelength calibration sources the reference spectrum from the literature and IUE archive is shown with uvot uv grism observations. The dotted line is a second observed spectrum. The X-axis wavelength is in Å, the Y-axis an arbitrary measure of flux (both counts, flux, and a rectified optical spectrum are shown). Note the good correspondence between uvot and reference spectra and strong emission lines. Some contamination of zeroth orders accounts for differences between the two uvot spectra in each panel. WR86 is a binary, which accounts for the UV flux rise; however the orbital velocities are small compared to the line width.

^{*} <http://www.zemax.com>

Table 11 (the tables have been placed at the end of the report, see section 13) lists the calibration data used for the UV grism nominal (wheel position = 200); Table 12 lists the calibration data used for the UV grism in clocked position (wheel position = 160; Table 13 lists the calibration data used for the V grism clocked mode (filter wheel position 955), while Table 14 lists the same data for the V grism nominal mode.

Notice that for the calibration of the V grism, and of the clocked UV grism, we had often a lenticular filter observation done right before *and* after the grism exposure. Such sandwiched observations allow an independent determination of the attitude drift during the observation sequence. Observations where the anchor point fell outside the detector area could sometimes be used.

7 Description of Analysis: Introduction

The UVOT has two grisms mounted on each filter wheel, a *visible* and *ultraviolet* grism, and each grism has two standard modes of observation: The *nominal* mode is where the filter wheel aligns the axes of the grism with the optical axes in the same manner as the lenticular filters are used. In the so-called “*clocked*” mode, the filter wheel is rotated less, thereby blocking part of the field of view. This reduces the number of stars in the field and allows the first orders to be less contaminated by zeroth orders of field stars. However, the reduced aperture affects the effective area due to vignetting.

The wavelength calibration is based on recalibrating the UVOT *Zemax* optical model using in-orbit observations. Since the model does not include the fiber taper (see Roming et al. 2004 for the instrument description), correction factors were determined by comparing to observations of Wolf-Rayet stars, WR4, WR52, WR86, WR121, and WR1 which show an abundance of well-defined spectral lines which are well matched with the spectral resolution. The spectra of these sources have been published in a number of papers, with the exception of WR 121. The fainter WR121 was required for the more sensitive V-grism, and line IDs were based on its spectral type. A comparison of the *Zemax* model with ground calibration data was also made which showed that the model fits well after applying a scaling factor.

First, the methods used to perform the calibration are discussed. Since there was a change in the grism calibration approach during the Swift mission, the old and new methods are outlined first, followed by a more detailed account of the new calibration methods. In section 10 this is followed by an assessment of how accurate the new wavelength calibration is, in terms of the knowledge of the anchor point of the wavelength scale and by comparing spectral line wavelengths in observed spectra with known wavelengths.

The position of the source in the field of view relative to the instrument boresight can be expressed in two angles on the sky (X_{phi} , Y_{phi}), measured along the image axes, hereafter called “sky angles”. These translate into the offset of the source to the boresight location on the detector (X_{ank} , Y_{ank}) through the focal length and pixel scale parameters as defined

in the TELDEF* file. The translation between the angles and the distance to the boresight position on the detector is done using the `uvotapplywcs` ftool. The angles are used as an index in the wavelength calibration file to look up the relevant parameters in the calibration table, like the anchor point, and the polynomial coefficients of dispersion for first and second order.[◊]

7.1 The anchor point

The reference point for the wavelength scale on the image will be referred to as the “anchor point”.

A source at a given position in the field of view is imaged at a certain position on the detector. That position varies slightly in the uvot lenticular filters (v , b , u , $uvw1$, $uvm2$, $uvw2$, wh) along with the boresight position in that filter. A source at the boresight will always produce an image at the same position on the detector for a given filter, while the boresight is common between all filters. In the spectrum a given wavelength will always lie at the same position. Thus the boresight can be defined for a particular wavelength. The position of a source anywhere in the FOV is then determined by position of boresight and angles along two axes between source and boresight.

There are two methods of determining the wavelengths available. The first one, the ‘old method’, was initially employed and has the anchor defined as the peak emission in the *zeroth* orders of weak stars in a grism detector image (detector file names are like `sw00012345001ugv_dt.img`). The second method defines the anchor at a wavelength of 260nm in *first* order for the UV grism, and 420nm in *first* order for the V grism. These wavelengths are those for which the grism design was optimized, and tend to be in positions somewhat like those in a lenticular filter on the detector. The new method can be used over the whole detector, whereas the original method relies on obtaining the zeroth order position.

7.1.1 New method with the anchor point in the first order

To find the anchor point in the first order, the following approach is used. The following steps describe this method:

- (1) The position of the anchor on the grism detector image is determined for sources at the boresight position in a lenticular filter. Since the boresight is common between all filters, this allows the determination of the anchor in the grism.

* e.g., `swugu0160_20041120v105.teldef` in the Swift UVOTA CALDB for the UV clocked mode; similar ones for the other grism modes.

◊ The anchor point in the first order should not be confused with the grism boresight in the Teldef file which is given for the zeroth order

- (2) The position of the anchor location on the grism detector image is determined using spectral lines for sources at various positions on the detector, while knowing the source location in the matching lenticular filter in relation to its boresight location. This allows the determination of the distortion. The source position offset from the boresight in the distortion-corrected lenticular filter image is used to derive the sky angles.
- (3) The measured distortion is compared to the distortion predicted from the Zemax optical model computation, and a bilinear or biquadratic scaling is determined from that comparison and used to correct the model.
- (4) The predicted anchor positions from the Zemax model as adjusted with the bilinear/biquadratic correction are used on the detector image as a function of the sky angles.

The advantage of using the lenticular filter to determine the reference to the sky position lies in the higher accuracy with which the positions are known in the lenticular filter, namely better than $0.5''$. The accuracy of the mapping is determined by the calibration described above, and the pointing accuracy during the observation. The in-orbit results are shown below in the discussion of wavelength accuracy.

In the case that there is no lenticular filter image taken together with the grism image (in the same Swift ‘mode’), the aspect correction can be made to the grism image using the `uvotgraspccorr` tool. This can be used to determine the position of the first order anchor in the grism image, though with reduced accuracy. All early grism observations were done without accompanying imagery in the lenticular filters.

7.1.2 The ‘old’ method with anchor point in the zeroth order

The following steps were taken to determine the anchor point in the zeroth order consistently. In the following of this section read, “peak emission in the zeroth order of weak sources” when referring to the “zeroth order”.

- (1) First the boresight was determined for the zeroth order. It is given in the TELDEF file of the Swift UVOTA CALDB.
- (2) The distortion of the zeroth orders was determined, meaning that after application of the distortion correction, distances on the sky scale linearly to distances on the detector. The zeroth order position distortion correction calibration product is called `swugrdist20041120v001.fits`.
- (3) An aspect solution based on the zeroth orders of weak sources in the image was implemented in the ftool `uvotgraspccorr`.

The result is a well-defined mapping between the sky coordinates and the anchor position of a source's zeroth order, providing a reliable reference point even when the source is bright and has a complicated, extended, and coincidence-loss affected zeroth order.

Tests have shown that an aspect solution can be found in over 90% of the images using this method. A frequent cause of failure is the presence of large extended objects in the field, or a lack of enough weak sources. In that case, it is recommended to find an aspect solution by hand, and edit the header keywords using the weakest sources in the image. The accuracy of this method is not well known. In the UV grism it is likely 5 pixels or more, and in the V grism it may be more. Because the typical dispersion in the UV grism is 3Å/pixel, in the V grism 6Å/pixel, this introduces a possible shift in the wavelength scale of >20 Å (UV grism) or >40 Å (V grism). Other possible systematic errors can arise if the majority of the weak stars used are not late type stars, as the calibration assumes they are. Stellar statistics nearly guarantees that to be a good assumption.

7.1.3 Finding the anchor point for the second order

The second order anchor point can only be measured for the uv grism and at offsets from the centre where the second order separates from the first so that it can be analyzed. Second order measurements were made using the strongest visible spectral feature as a temporary anchor, which was the 1910 CIII] line. The position of the second order anchor was determined referenced to that of the first order anchor from the rotated detector images, as a distance in pixels. Similarly, the dispersion was determined from line features mainly in the 1750-2600Å range, since at longer wavelengths there is order overlap, until at the longer wavelengths only the second order remains. However the PSF is very broad at such long wavelengths, so the usefulness is limited to a consistency check. The work is still in progress, as some issues remain in finding a good overall fit.

7.2 Dispersion

The dispersion was determined in different ways for the first and second anchor point methods. The first method will be briefly described only, since it is being superseded by the second method.

7.2.1 dispersion with the anchor in the zeroth order

The distance from zeroth to first order is of the order of 200 pixels in the uv grism which is included in the dispersion expression. It should be noted that the dispersion was determined using this method for the default positioning of the grism spectrum only, and can be found in the calibration database^{*}. If the spectrum falls farther than a few hundred pixels away from the centre, the distance between the first and zeroth order changes, as well as the dispersion. This limits the usefulness of this calibration. Blue sources have a strong second order starting affecting the spectrum around 275nm, although that usually

^{*} swuugrism20041120v102.fits and swuvgrism20041120v102.fits

does not become noticeable until 295nm. Sources with a red spectrum have second order contamination starting at longer wavelengths. For a F0V around 420nm, for a K0 there may not be any second order contamination. The calibration sources used for determining the wavelength calibration were not documented publicly. The dispersion relation leads to wavelength errors less than $\sim 30\text{A}$. The error is dominated by the anchor position accuracy.

7.2.2 dispersion with the anchor in the first order (new method)

In order to determine the dispersion, calibration spectra were taken at various positions on the detector. The data were discussed in section 0. The following steps were taken to ensure a consistent approach.

- (1) The slope of the spectrum on the detector image is always the same for the same filter wheel position. It was determined using the slope of the spectrum as computed at the anchor point of the spectrum using the Zemax optical model. This angle varies by a few degrees over the detector. This provides a consistent approach that is valid for most of the detector.
- (2) The image was rotated over the angle so that the spectrum is dispersed mainly along the x-axis. However, in the uv-grism the spectrum is curved and the orders can show slight displacements normal to the dispersion depending on where on the detector the spectrum lies.
- (3) The curvature of the spectral orders was determined and parameterized in polynomials. The polynomial coefficients were then fitted to bilinear, biquadratic, or bicubic functions for interpolation as function of the anchor position.
- (4) The spectra were used to measure positions of known features, and to determine the dispersion. The dispersion computed in the Zemax optical model was then scaled using a best fit to the measured dispersion. The scaled dispersion of the Zemax optical model was used to produce the wavelength calibration file which provides the dispersion as coefficients of a polynomial on a 28x28 grid over the detector. The wavelength calibration files are:

swugu0160wcal20041120v001.fits, swugu0200wcal20041120v001.fits,
swugv0955wcal20041120v001.fits, swugv1000wcal20041120v001.fits.

The method used to determine the dispersion is the same as the method used to extract the spectra using the new python software[†]. Although the dispersion angle from the model of the spectrum on the detector matches the direction of the different orders on the image, the individual orders may show some curvature and appear to lie at a different angle depending on the anchor position.

[†] <http://www.mssl.ucl.ac.uk/~npmk/uvotpy>

8 The preliminaries to the wavelength calibration

8.1 Use of the Zemax UVOT optical model

The *Swift* UVOT optics was designed with the help of a *Zemax* optical model. The model includes telescope optics, and models for the lenticular filters and the grisms. It does not include the fiber taper optics, nor the CCD, i.e., no correction for any multiplication factor or distortion due to them, hence the correction to the pixel scale in the model has to be worked out.

Our approach has been to use the distortion determined for the lenticular filters, thereby assuming that the distortion seen in the lenticular filter images is mostly due to the fiber taper optics, and that the contribution to that distortion from the lenticular filters is relatively small. This has been mostly borne out by the calibration with only a small distortion correction remaining to be made at the end in the form of a scale factor.

Grism data are initially formatted into 2048x2048 arrays in a RAW grism image. The standard *Swift* UVOT processing corrects the RAW grism image using the distortion as determined from the *lenticular* filters, to produce the detector (DET) image (e.g., `sw00056950007ugu_dt.img`). The RAW and DET images use different coordinate systems. The RAW image coordinates are in pixel numbers measured from the bottom left corner, whilst the DET coordinates the center of the image is the reference and the unit is in mm. In the *TELDEF* calibration file, the DET coordinates have been used after conversion to pixel coordinates using a scale factor of 0.009075 mm/pix with the centre of the image at (1100.5,1100.5), which are called DET-pixel coordinates for clarity. This means that the image is embedded in a larger undefined array. Using just the defined image array with the first pixel in the bottom left corner is useful when making measurements, so this is used rather frequently, and referred to as the *image* coordinate or *physical* coordinate system. For details on the coordinate system used in *Swift* UVOT, see the documentation for the *TELDEF* File, and the *TELDEF* file headers.

8.2 Determination of the boresight position for the grism image in first order

Since the optical model is not a complete representation, the model needs to be aligned with the observed boresight consistent with the lenticular filters. This means that first the boresight position needs to be determined at the anchor point for each grism mode. This was done using the strong emission lines in the WR stars close to the anchor, like the lines at, for example, 2398, 2405, 2530 Å for the 2600 Å anchor in the uv grism, and the 4649 Å line for the 4200 Å anchor in the V grism. Four observations were taken for the uv nominal mode, six for the uv clocked, seven were used in the V nominal, and clocked modes, attempting to position the source as closely to the boresight in the accompanying lenticular filter observation as was possible. Therefore, the grism spectrum observation directly followed, or was directly followed by an observation in the *uvw1* or *uvw2* filter,

which can then be used to determine the source offset from the boresight, since the boresight for the lenticular filters is known.

The spectral lines in the image were identified and their position measured to determine the position of the anchor point by interpolation and extrapolation, using the dispersion in an iterative fashion.

Grism mode	Anchor point wave length in Å	Boresight position in image (physical) coordinates	Boresight position in DET coordinates	Uncertainty in x and y image coordinates	Filter wheel position
UV clocked	2600	1025.1, 944.3	1129.1,1022.3	5,5	160
UV nominal	2600	901.5,1001.7	1005.5,1079.7	2,2	200
V clocked	4200	1036.7, 951.6	1140.7,1029.6	3,3	955
V nominal	4200	942.3,1020.3	1046.3,1098.3	1.9,3.9	1000

Table 1: Boresight positions in the first order grism modes

The uncertainty in the boresight position is about 5 pixels in the uv clocked mode because none of the observations approached this point closer than 22 pixels.

8.3 Determination of the scale factor for the model in the dispersion dimension

The *Zemax* model calculation provides for each input angle (which is similar to the sky angle, but on the optical model coordinate system) the position of the peak intensity at specified wavelengths in five orders: the zeroth, first, second, third and minus first orders. For the spectra taken near the boresight position, the predicted and observed wavelength as a function of pixel distance were compared. It was found that the model dispersion needed to be scaled to fit the observations. For the uv nominal a simple scale factor 0.960 provides an acceptable fit over the whole detector. Comparison of the nominal uv grism scale factor to the pre-launch ground calibration gave the same factor as found in-orbit (see 8.6).

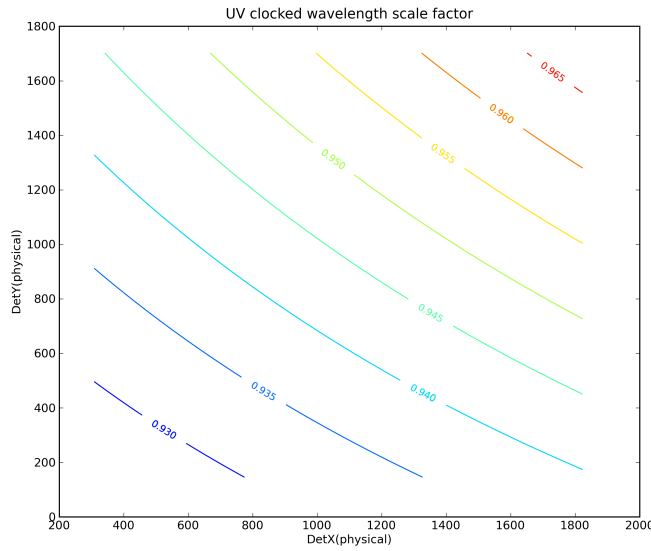


Figure 2. The scale factor in the uv clocked grism to convert the Zemax model wavelength scale to the observed scale.

For the uv clocked grism, a good fit required a bilinear fit to the observed scale factors, which ranges from 0.93 – 0.96, see Figure 2.

In the nominal V-grism, the scale factor for the dispersion at the centre of the detector is found to be 0.967 ± 0.02 , but there is some variation over the detector, as shown in Figure 3. In the V clocked grism mode the scale factor is about 0.89 ± 0.015 , see Figure 4.

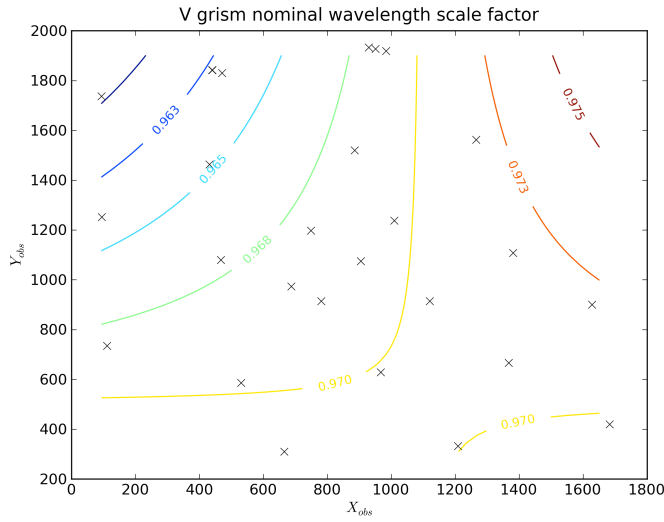


Figure 3. The scale factor for the dispersion for the V nominal grism. The crosses are the position of the anchor points of each of the calibration observations.

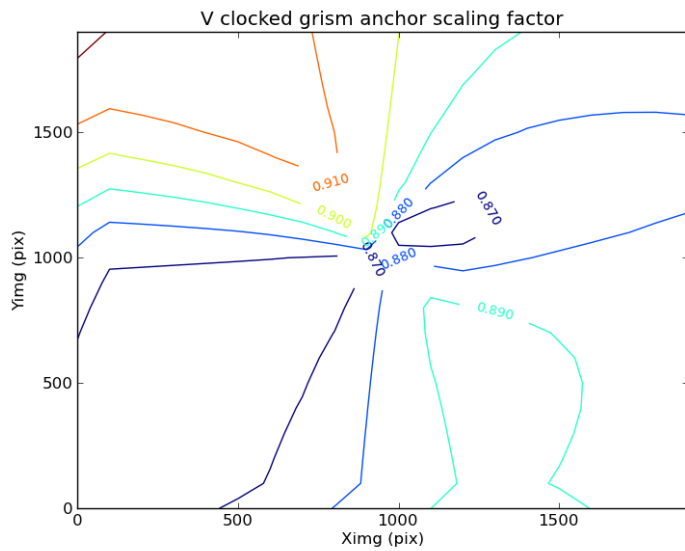


Figure 4. The anchor scale factor for the V clocked grism.

8.4 The anchor point position in the calibration image

For all calibration observations made with spectra positioned at offsets over the detector, the anchor point position was determined as outlined in section 7.1.1 above.

As mentioned in section 8.1, the distortion correction that is applied to the ‘detector’ image was that determined from the ground calibration in the lenticular filters (see Breeveld et al., 2010). Though it removed the distortion from the fiber taper, additional distortion may be expected from the grism optics and the correction may not apply as well for the grisms. This is considered to be the main reason that we need a small bilinear or biquadratic correction to the anchor positions from the Zemax model.

The unscaled Zemax model positions for first order anchor points were found to be close to the observed ones, with increasing distances to the edges of the detector. This is likely due to using an inaccurate distortion correction, and to first order is a simple scale factor. The details are given in section 10.

The scale factor is different for the clocked and nominal modes, and for the uv and V grisms, and of the order of a few percent. The observed anchor point data for the uv clocked grism is better defined than that for the nominal grism since the uv clocked data had lenticular filter data both before and after the grism exposure which allowed us to interpolate for attitude drift. The anchor position scale factors were applied to the Zemax models in the calculation of the anchor positions for the wavelength calibration files.

8.5 No Anchor point adjustment to account for the boresight point drift.

The grism calibration determines the anchor point by mapping the position of a source in a lenticular filter image to that in the grism detector image. That mapping is independent of any changes in the boresight position, since as the boresight and all source positions move in the one filter it moves also in the others, or, looking at it in another way, the mapping is an instrumental property that is fixed by the hardware.¹

8.6 Fitting to ground calibration data [nominal UV grism mode only]

Before launch, in November 2002, the complete UVOT instrument had a ground calibration at the NASA Goddard Space Flight Center. The calibration of the grism could only be done for one position, along the central axis which corresponds closely to the boresight of the instrument. Although ground calibration at some clocked positions was done, the actual optimum in-flight clocked filter wheel position was quite different, and therefore only those for the nominal position are useful. The light source used was a

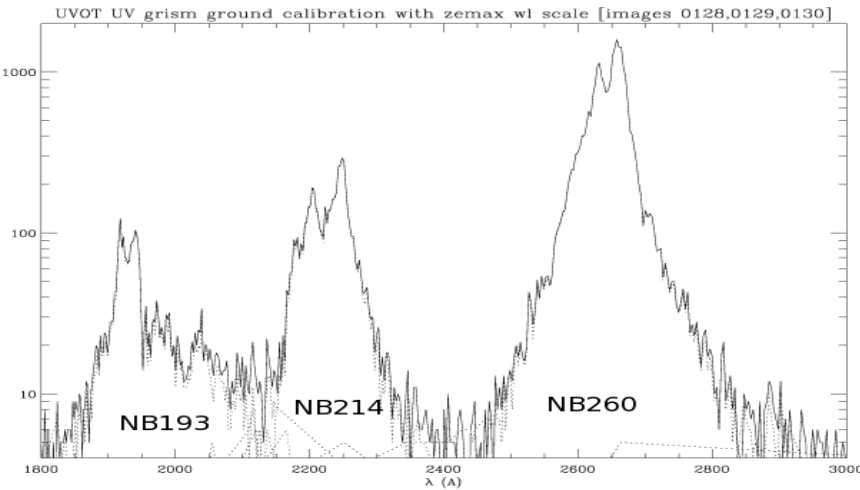


Figure 5. Ground calibration. Combined in one figure are three Pt/Cr/Ne Lamp observations with the measurements from the three broad-band filters along the dispersion direction in the first order. The observations were taken in sequence with the source on-axis. The dotted lines show the individual filter contributions. The strongest lines visible are at 1930, 2175, 2203, 2246, 2631, and 2660Å.

Pt/Cr/Ne Lamp, while several broadband filters could be inserted into the light path entering the telescope. A combined spectrum was made and is given in Figure 5.

¹ The change in boresight position over time also affects the scaling factors used, but can be disregarded in practice since these change slowly over the detector face.

In order to fit the observations and the calibration, the observation was found to have a slightly different angle for the dispersion plane, at an angle of about 68.8° , while the design was 65° . The correction of 3.8 degrees was incorporated into the Zemax model calculations. The origin of the extra angle lies most likely in the mounting of the grism into the hardware. The scale factor derived from the measured line positions in the ground calibration is consistent with the factor 0.960 that was derived in the in-orbit calibration. The Zemax model also predicts quite well the zero and second order positions measured in the ground calibration once the scale factor is taken into account.

9 The wavelength fit of spectra across the detector

The spectra are not dispersed with the same spectral slope across the detector. The Zemax model predicts the variation of the slope over the detector. The predicted spectral slope at the anchor point was successfully used for extracting the spectra. The detector image was rotated around the anchor point by the spectral slope angle from the calibration file (about 151.2 (uv nominal), 144.5 (uv clocked), 148.1(v nominal) and 140.8(v clocked) degrees). A strip containing the spectrum and background was extracted. The predicted anchor point was generally not centered exactly on the spectrum (mainly due to curvature of the spectrum), so a projection of the anchor point to the peak of the crosscut spectrum was made. Then the wavelength was computed using the interpolated model prediction. Out of necessity this process was iterative, using first the scaled Zemax model, and then using the initial results to determine the scaling better.

The error to the wavelengths arises from two factors. The first is due to the accuracy of the predicted anchor position which affects all wavelengths by a shift in the position of the reference wavelength. The second factor is the internal consistency of the dispersion, which depends on the accuracy of the scaled Zemax model.

The average offset of the anchor point in the nominal uv grism calibration was about two times larger than in the uv clocked calibration, and the V-grism calibrations, which is probably due to the improved observed anchor point positions that were obtained when the later grism observations were sandwiched between lenticular filter observations using the new observing modes*. This resulted in an overall improvement of the accuracy of the location of the anchor point over the nominal calibration. See also section 8.4.

The spectra of WR52 and WR86 show several well-defined carbon lines and some weak He lines at 1909, 2297, 2405, 2530, 2906, 3409, 4069, 4649, and 5803 Å. Those of WR121 (used for the V grism,) show a multitude of lines, notably lines of He I, C II, III, IV at 3609, 3733, 3889, 3919, 4650, 4786, 4859, 5016, 5141, 5696, 5801, and 6580 Å. Second order lines were not readily found, though some offset uv-grism spectra of WR52 show uv lines like CIII] 1909, the 2297 and 2405 lines in second order.

Using the new wavelength calibration, the spectra are extracted again. The well-identified lines in the spectrum are then used to determine the accuracy of the predicted wave-

* http://www.mssl.ucl.ac.uk/swift/pt_release15.tab

length. When the results were examined, the anchor position did not always line up with the initial anchor position. Since this gave another, more accurate way to correct the anchor positions, an iteration was done to improve those. After implementation of the improvement, the remaining error in wavelengths was found to be about 3 and 5 pixels (1σ) in respectively the uv nominal and uv clocked calibration, and about 3 and 4 pixels in the V nominal and V clocked grism modes (in the dispersion direction), neglecting outliers. Outliers can be attributed to spacecraft drift that occasionally happens during an observation. Indeed, the outliers occur all over the detector and show no discernable pattern.

Although the error in the anchor point in the clocked uv grism calibration is much smaller, the error in the overall dispersion relation is much better in the nominal uv grism, leading to a better wavelength for the nominal grism. In the uv clocked calibration, the observations with the anchor point at high X, where $X(\text{physical}) > 1500$, show increasingly large wavelength errors which may be due to incorrectly converting the model to the calibration file, and needs further investigation.

10 Error analysis of the new calibration

In this section the errors are determined for the anchor position, and wavelength scale. Parts of the earlier discussion of the calibration are repeated here for clarity, and some further details are given. The section discusses each filter mode in sequence. For each filter mode, first the determination of the anchor point and the wavelength scale offset are discussed, followed by the determination of the wavelength accuracy after re-extracting each calibration spectrum using the new wavelength calibration file. Some representative results are displayed in graphical form.

10.1 UV Nominal Grism

The spectrum in the image was extracted and spectral lines were identified. The locations of the lines on the image were then used to determine the location ($X_{\text{obs}}, Y_{\text{obs}}$) of the anchor point on the image.

The input angle ($X_{\text{phi}}, Y_{\text{phi}}$) of the input ray from the boresight was determined using the image in the lenticular filter. Sometimes the source is very bright in the lenticular filter, therefore the procedure used was as follows: (1) the $uvw1$ sky image was aspect corrected and checked; (2) the source position in RA, DEC (J2000) and header information of the $uvw1$ image was then used to determine the location of the source on the detector in DET(mm) coordinates[▼], which was checked using DS9[◆]; (3) after conversion of the DET coordinate to pixels (using the conversion factor 0.009075 mm/pixel), the pixel

[▼] using the Ftool `uvotapplywcs`

[◆] DS9 is part of WCSTOOLS by Doug Mink at SAO

difference in X and Y on the detector was determined from the offset of the known boresight of the lenticular filter; (4) the difference in pixels was used with the lenticular filter scale factor of 0.502"/pixel to determine the input angle. This can be done since the image has been distortion-corrected. For those observations where the grism exposure was sandwiched between exposures in two lenticular filter images, the mean input angle was used. Drifts in attitude when the grism was sandwiched between the two lenticular filter observations were found to be $\sim 6.4 \pm 2.7$ pixels in 500s, which translates to about 3.2" in 500s.

The input angle was used to do a lookup of the parameters using bilinear interpolation in the grid of data in the calibration file prepared by us, to determine the predicted anchor position (X_{ank} , Y_{ank}), the angle θ , which describes the angle of the first order on the detector image near the anchor point and the dispersion coefficients C_{1j} for the wavelength scale. The spectrum is extracted after rotation over the angle $180-\theta$.

The wavelengths can be found from the polynomial formula:

$$\lambda = \sum_{j=0,n} C_{1j} p^j$$

With λ the wavelength in Å and p the pixel-distance to the anchor point along the direction defined by the angle θ . Similarly, for the second order where the coefficients are C_{2j} .

The second order dispersion is referenced to the anchor of the *second* order, and the second order anchor is another calibration product provided in the wavelength calibration file. The second order position and dispersion has been derived from the optical model as described in section 9, but has so far only partially been verified against ground calibrations at the boresight, an inspection of a spectrum of RS Oph in outburst (clocked uv grism), and spectra taken in the uv grism at large offsets.

The zeroth order dispersion as predicted by the optical model is hyperbolic with a very extended uv tail and most light redward of 4000Å in a single peak. This has been verified to some extent with the ground calibration at the boresight position, the occurrence of a spectral line at $\sim 1730\text{Å}$ in RS Oph, and spectra from WD1657+343. The zeroth order can be used to determine a rough magnitude estimate[▲].

Using the observations listed in Table 11, in Table 2 the measured and calculated anchor position and input angle have been listed for the uv nominal grism using the positions in the image. The measured positions on the image are related to the DET-pixel coordinates by adding (104,78)^{*} to the coordinates for $(X,Y)_{obs}$ and $(X,Y)_{ank}$ in the table.

[▲] see "Zeroth order effective area and efficiency" document at
http://www.mssl.ucl.ac.uk/~npmk/Grism/fluxcal/zeroth_order_ea_and_effcy.pdf

^{*} Using the FITS header, this comes from (1100.5-CRPIX1,1100.5-CRPIX2)

Observations with ID 28 and 30 were too close to the edge of the detector to find an anchor point by simple bilinear interpolation. No extrapolation was attempted, although the initial calibration did use these data.

Observed and predicted anchor positions on the image and the input angle of the incoming ray – UV grism nominal.						
ID	X_{obs}	Y_{obs}	X_{phi}	Y_{phi}	X_{ank}	Y_{ank}
1	905	995.1	0.00066	-0.00068	904.5	995.5
2	917.5	992.1	0.00250	-0.00176	916.2	988.7
3	916.9	991.3	0.00232	-0.00144	915.1	990.7
4	923.2	999.0	0.00306	-0.00051	919.7	996.7
5	877.4	1009.0	-0.00318	0.00142	880.1	1008.6
6	947.2	1021.2	0.00668	0.00264	942.5	1017.0
7	801.9	1073.9	-0.01642	0.01086	796.4	1067.8
8	895.9	1116.8	-0.00167	0.01752	889.3	1111.2
9	879.5	978.9	-0.00419	-0.00405	874.0	973.7
10	1046.5	767.9	0.02144	-0.03827	1038.4	756.0
11	1068.0	769.1	0.02609	-0.03729	1068.0	762.4
12	1135.3	1167	0.03484	0.02377	1121.0	1153.3
13	1130.1	1190.8	0.01959	0.02490	1134.6	1185.7
14	809.3	1155.4	-0.01708	0.02184	801.4	1151.6
15	724.3	1262.4	-0.02740	0.04051	737.1	1274.2
16	667.4	779.9	-0.05671	-0.04050	661.2	772.8
17	646.0	851.1	-0.03982	-0.02373	657.7	856.1
18	1162.1	685.0	0.02328	-0.05101	1162.0	700.0
19	1491.7	668.5	0.09335	-0.05127	1502.2	673.3
20	1102.3	1082.3	0.01582	0.01082	1110.9	1095.8
21	1403.5	1217.1	0.06141	0.02834	1402.7	1209.7
22	758.5	1598.0	-0.03820	0.09105	769.7	1599.6
23	1028.7	1652.4	0.00257	0.09773	1026.9	1645.9
24	540.4	1538.9	-0.07202	0.08193	558.1	1538.4
25	691.7	1499.9	-0.03133	0.07736	703.1	1487.4
26	237.3	1672.7	-0.10971	0.10977	219.4	1680.5
27	489.2	1786.6	-0.08311	0.11945	491.5	1772.2
28	62.1	1228.0	-0.15208	0.03472		
29	307.7	1349.6	-0.11069	0.05035	317.3	1335.1
30	86.0	703.3	-0.12996	-0.04338		
31	373.5	824.1	-0.09934	-0.03206	387.3	814.6
32	444.2	368.5	-0.09012	-0.09966	448.2	382.4
33	702.4	409.5	-0.04824	-0.09609	711.0	407.4

Table 2: anchor positions in the uv Nominal grism

10.1.1 Accuracy of the anchor point for the UV nominal grism calibration

The position of the anchor points for all uv nominal observations in detector physical coordinates are shown in Figure 6. As can be seen, the measurements are spread over virtually the whole face of the detector, so the wavelength accuracy of the anchor point position applies for the whole detector. Near the centre of the detector, the prediction of the positions of the anchor points are slightly better than near the edge. The error is measured in terms of wavelength offset ($\Delta\lambda$). There were 5 data points with a high value for $\Delta\lambda$ at various places on the detector (see Table 3) which have observations that are suspected to have drifted during the observation. Three observations were too close to the edge to be used.

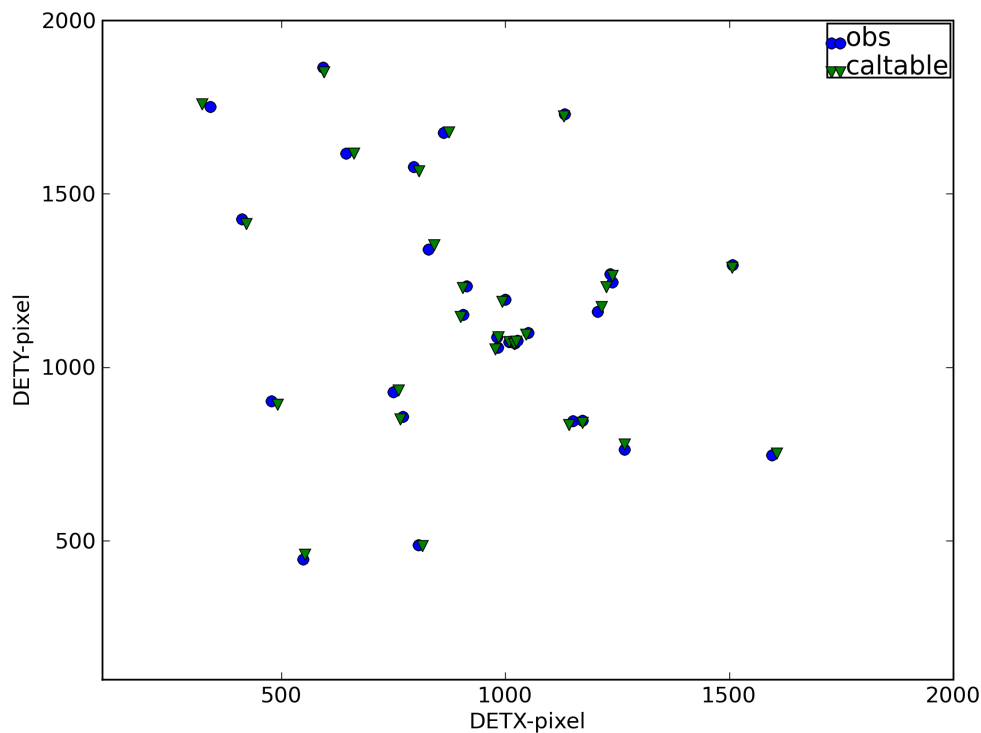


Figure 6. The observed anchor points are blue, and the ones derived using the calibration file are green triangles. The coordinate system is the DET coordinates converted from mm to pixels and the centre at [1100.5,1100.5].

10.1.2 Accuracy of the wavelengths using the uv nominal grism calibration file

In the discussion of the calibration in section 9 above two error sources for the wavelength accuracy were introduced. The first error is how accurately the anchor position of the wavelength scale can be determined from the sky position of a source, or equivalently, from the position in an image taken in a lenticular filter together with the grism in one observation sequence. The second source of error is how accurate the wavelength scale is over the whole range from 1750-6500 Å, or whatever part falls on the detector.

The accuracy of the determination of the anchor position using the calibration file has been discussed in section 10.1.1. We now consider the accuracy of the wavelength determination over the whole range, by comparing measured line positions in the extracted spectrum to their predicted positions. The coefficients of the dispersion polynomial from the calibration file were interpolated using the input angle to derive the dispersion relation for each observation.

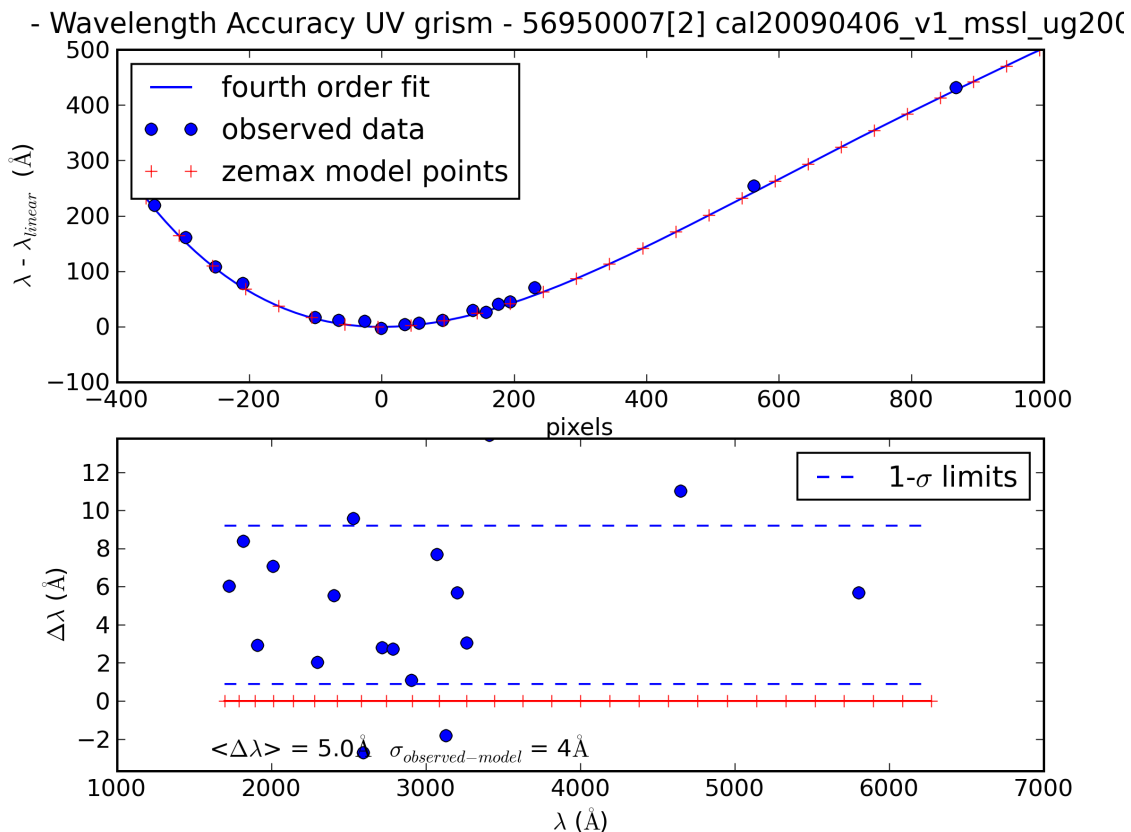


Figure 7. Wavelength accuracy uv grism spectrum. This figure is for a spectrum (Table 11 ID=3) falling nearly on top of the boresight (the centre). The top panel shows, as a function of pixel distance to the anchor at 2600 Å, the residual wavelength difference

after subtraction of the linear dispersion term which by definition gives zero at the anchor position. The crosses follow the dispersion relation; the dots are measured from the image; and the blue line is the best fit through the model. The bottom panel shows the difference of the observations from the model. The blue lines have been placed at one-standard deviation from the mean wavelength offset.

The spectra were extracted by using the calibration file cal20090406_v1_mssl_ug200.fits.

Any inaccuracies in the position of the anchor show up as a common shift of the observed differences in wavelength (bottom panel); inaccuracies in the form of the dispersion relation will show as a gradual difference of the observed points from the model points (+ signs) or the polynomial fit (the line) in the top panel. Inaccuracies in the measurements of the wavelengths will result in a spread in the lower panel. Dashed lines indicate the one standard deviation error.

It can be seen that the fit in Figure 7 is quite good, and the mean offset of the wavelength differences which is due to inaccuracies in the anchor position is here 5.0 Å, which is about two pixels. The spread in the wavelength differences is of similar magnitude as the line widths in the spectrum. Therefore the spread is mainly due to errors made in measuring the line positions.

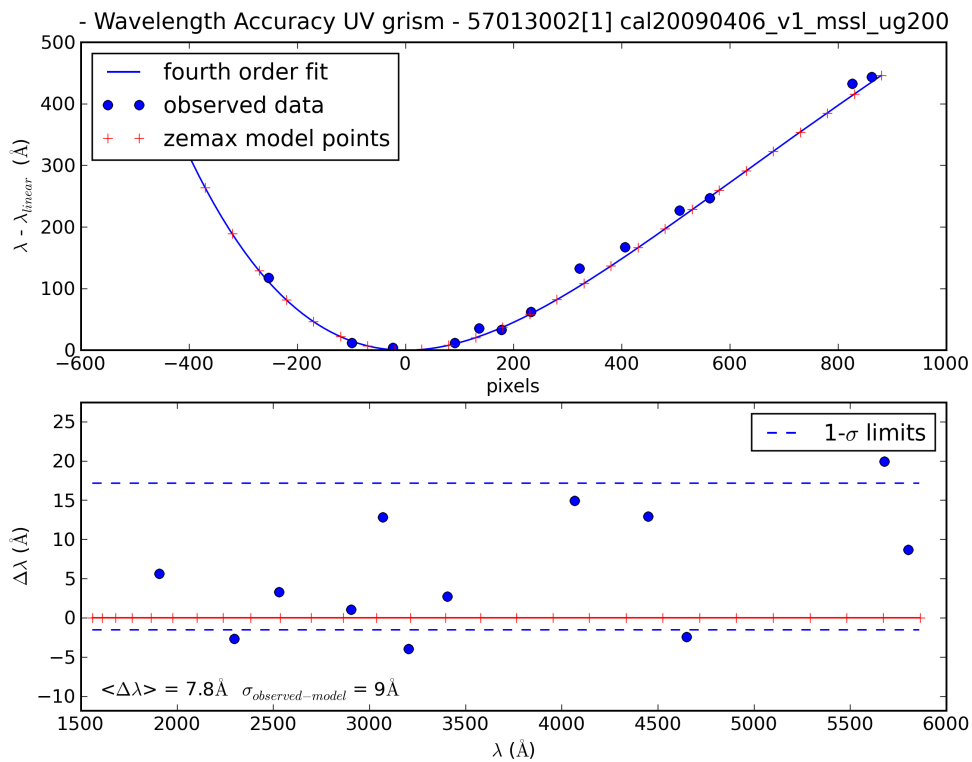


Figure 8. uv nominal wavelength accuracy. Same as Figure 7 but for (ID=8 in Table 11). This observation is at a distance of 111 pixels (about 1 arcmin) from the boresight (centre).

The following figures are with anchor points located at varying distances from the boresight. The dispersion relations for those points are different from those at the boresight. Figure 9 shows a slight trend in the disagreement between the observed and predicted wavelength. However, the difference is smaller than 10 Å. The largest difference in dispersion between model and observations occurs very close to the detector edge, and is still reasonably small. With that we mean that these inaccuracies are small compared to the uncertainty from the anchor position and relative to the resolution.

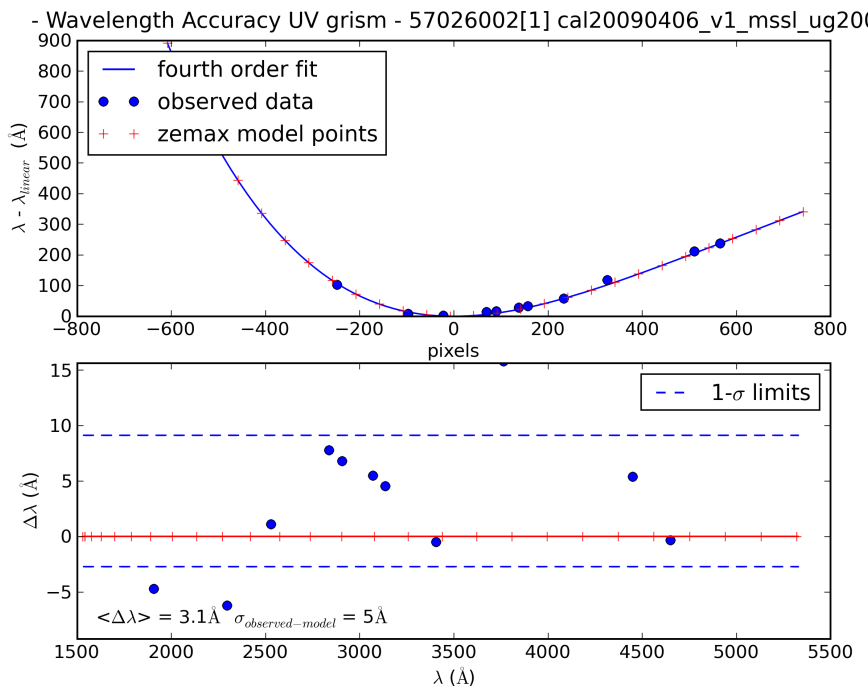


Figure 9. uv nominal wavelength accuracy. Same as in Figure 7, for a different position (ID=33 in Table 11).

The accuracy found from these fits includes the uncertainty in anchor position, so a comparison to Figure 13 is useful.

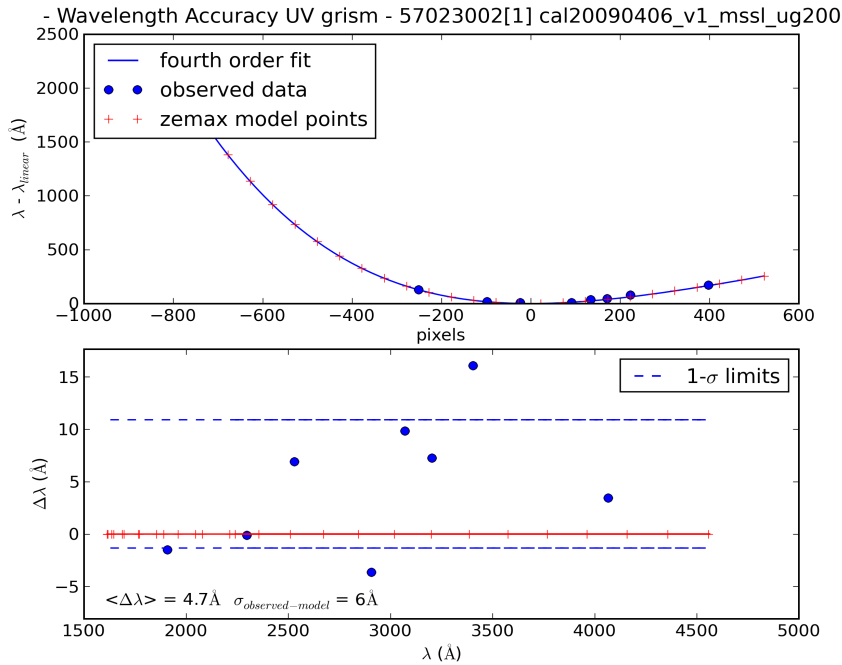


Figure 10. Same as in Figure 7, for a different position (ID=27 in Table 11).

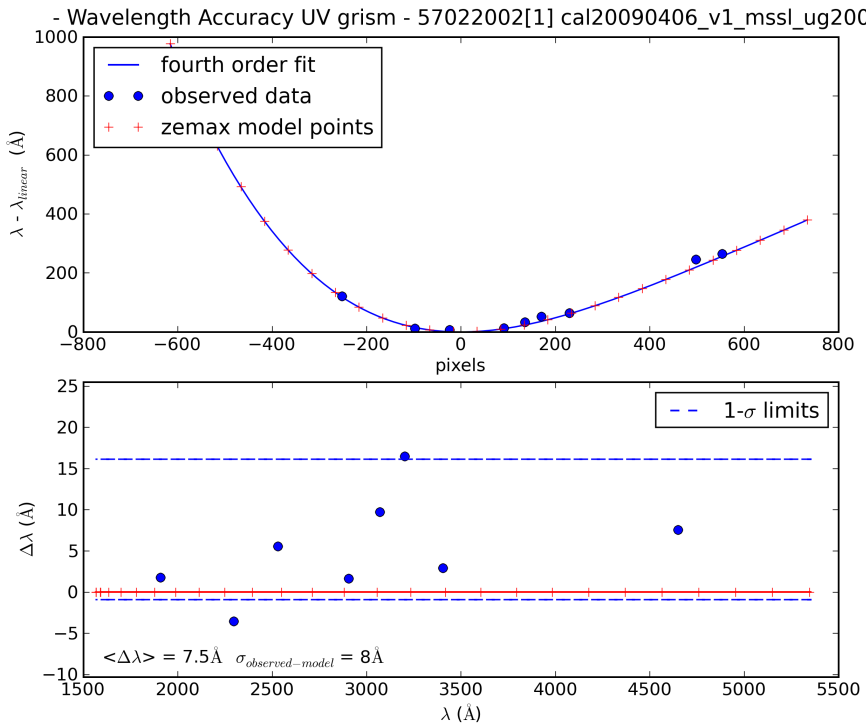


Figure 11. Same as in Figure 7, for a different position (ID=25 in Table 11).

Nominal grism			
ID	Anchor normal offset to spectrum in pixels	Anchor wavelength error (Å)	Standard deviation of spectral lines used (1-sigma) wavelength error (Å)
1	0	-3.4	8.6
3	-2	-20.4	7.6
4	-4	-25.4	8.0
2	-4	-13.3	5.8
9	-8	-9.6	3.6
6	-5	-14.7	9.8
8	-8	-11.0	9.7
7	-8	-16.2	9.7
14	-24	-27.8	8.2
20	15	-14.0	6.9
12	-19	-38.0	9.1
10	-16	18.6	14.0
11	-7	-2.3	4.6
17	-4	14.1	5.1
13	-2	2.5	5.4
15	-5	3.6	4.9
16	-23	-7.4	6.3
18	12	38.8	7.8
25	-6	4.6	8.2
21	-6	2.3	8.2
22	8	-26.3	13.8
33	-1	8.8	6.4
24	8	-25.2	14.6
23	-5	4.6	8.2
29	-9	4.2	6.0
19	9	11.3	12.4
32	10	-7.3	7.4
27	-10	-10.8	5.3
26	0	-26.3	10.6

Table 3: Wavelength errors by spectrum in the uv Nominal grism

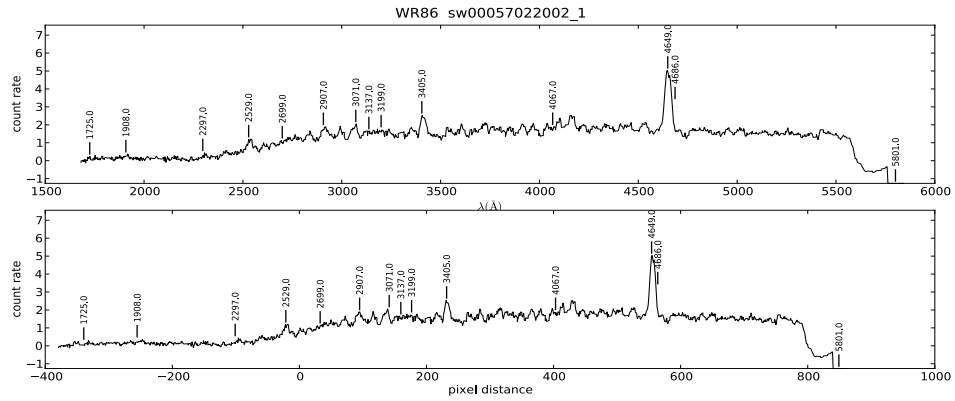


Figure 12. The figure shows the spectrum used in Figure 11 as a function of wavelength in the top panel, and as a function of the distance to the anchor in pixels in the lower panel. Line identifications are given at the positions calculated using the dispersion relation in the top panel. Shifts would indicate an inaccurate anchor position. For all spectra these plots were made and used to analyse the accuracy of the calibration.

In Table 3 the results from the spectral fits are summarized. These are the distance of the predicted anchor point to the spectrum, measured normal to the dispersion (anchor normal offset), the wavelength shift due to the error in the anchor position, and the standard deviation of the wavelength errors of the lines used.

Looking at the second inset "accuracy", and disregarding the systematic wavelength scale offset from the top left inset, wavelengths from the dispersion relation are found to typically fall within 14 Å (about 4 pixels) of the correct value. The "accuracy" is the RMS dispersion of the dispersion errors over the whole range as shown in the accuracy plots below in more detail, and not the error themselves. The variation of the accuracy of the dispersion relation over the detector can be seen from the contour plot Figure 14. The contours are the RMS values of the wavelength errors of known lines in the calibration spectra. There is only a small variation over the face of the detector present, with the largest discrepancies in the top left and bottom right corners. This can possibly be improved by applying a bilinear correction as a function of the detector position to the Zemax model dispersion constants. In the uv nominal grism, a constant was used. In the other grism modes which were done later, a bilinear or biquadratic correction was used.

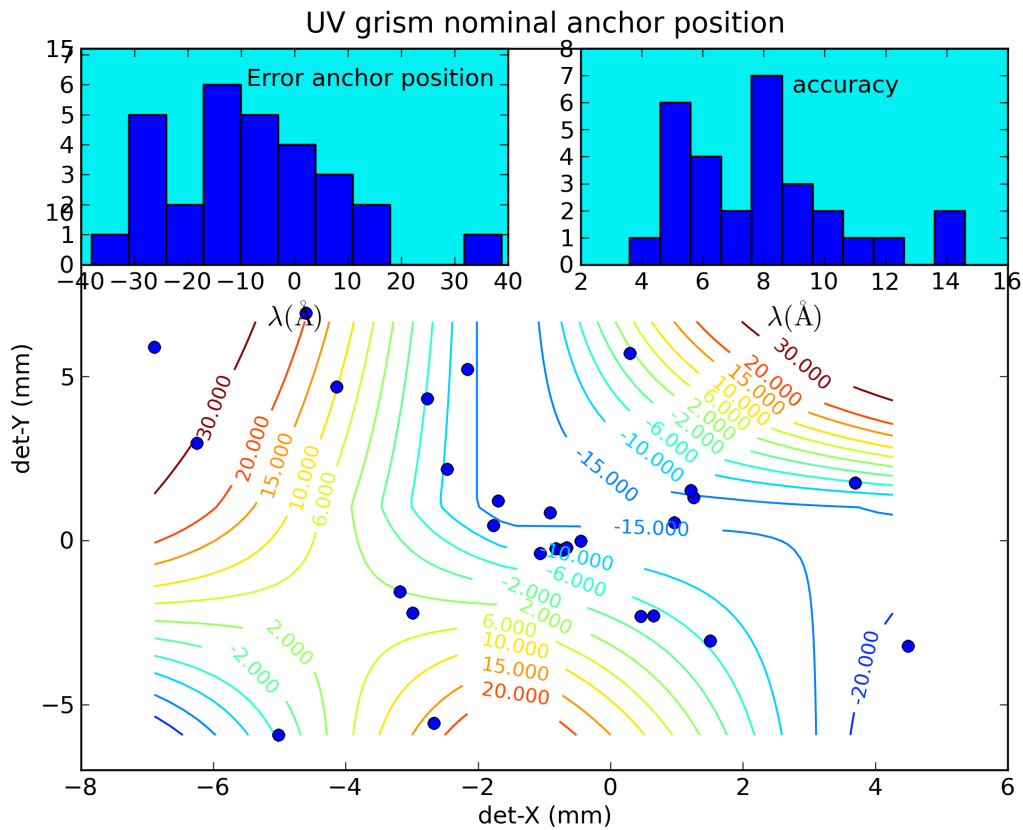


Figure 13. Summary of error and accuracy in the nominal wavelength calibration. The inset in the top left corner shows that at most times the anchor point that was predicted using the lenticular filters taken just before and after the observation, for the first calibration has a systematic offset of -8.0 \AA averaged over the calibration observations (blue dots). Ignoring the systematic offset, the anchor is found with a spread of 33\AA . The contours give a better picture of where the calibration for the anchor position results in an offset in the wavelengths. In the corners and near the edges, only a few observations were available for the calibration, so the values should be taken as an indication of the size of the error, rather than an accurate value that can be used to improve the wavelength scale knowledge.

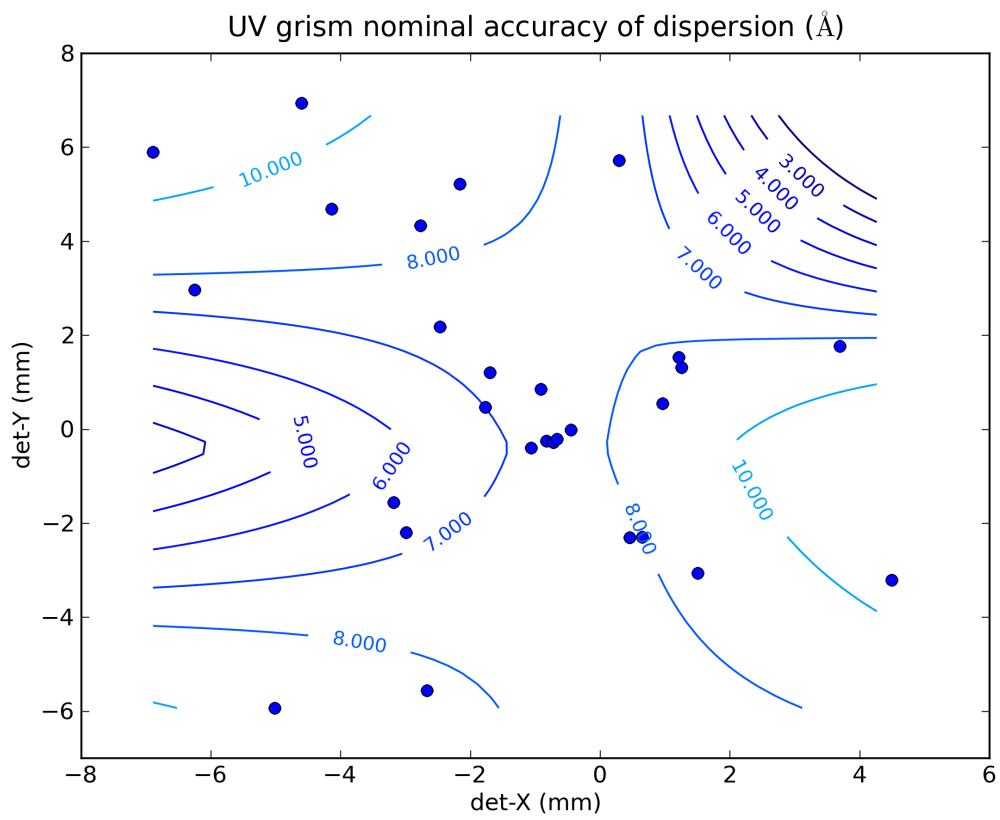


Figure 14. A contour plot to show the variation of the accuracy of the dispersion relation over the detector. Contours are in \AA .

10.2 UV clocked grism

The analysis was done similarly to the uv nominal grism; look there (section 10.1) for a more complete discussion.

The observations for the clocked uv grism had a better coverage of the detector than the nominal uv grism observations. The difference between observed and predicted (unscaled Zemax model) positions was more regular than in the nominal uv grism. In particular, some observations with anchors at high XDET were made. These spectra with anchor points at large X have no zeroth order, and some miss the uv part of the spectrum below 2300Å.

The anchor positions for the corrected Zemax model and the observed positions (see Table 12) have been put in Table 4 and are shown in Figure 15.

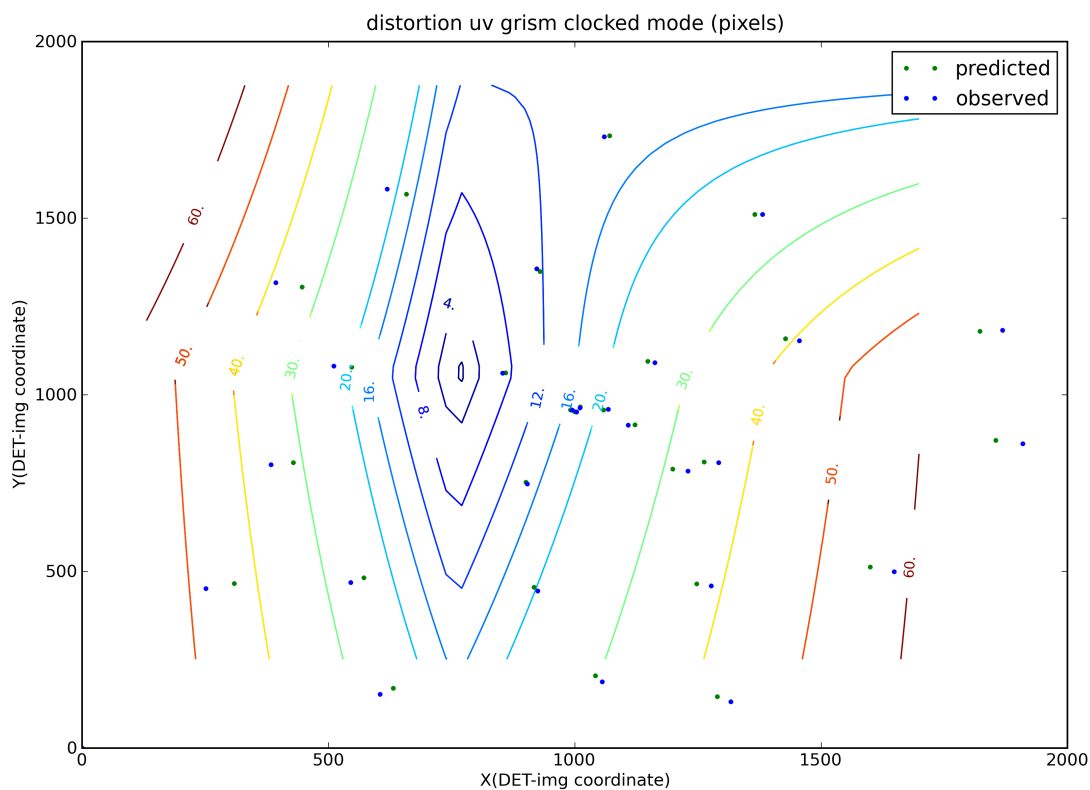


Figure 15 Prior to correcting the zemax model. The observed position of the anchor points from spectra in the clocked uv grism and the unscaled zemax model. The axes

are the physical X, Y detector coordinates. A bilinear interpolation was made to derive contours of the offsets between the observed and predicted anchor positions (in units of pixels). This was the basis for the correction to the Zemax model anchor positions.

Observed and predicted anchor positions on the image and the input angle of the incoming ray – uv grism clocked.						
Spectrum ID (from Table 12)	X_{obs}	Y_{obs}	X_{phi}	Y_{phi}	X_{ank}	Y_{ank}
34	1198.6	790.3	0.03095	0.02534	1207.5	790.4
35	1011.3	965.9	-0.00227	0.00284	1005.3	965.8
36	1122.0	915.3	0.01260	-0.00506	1095.6	917.5
37	999.7	952.6	-0.00332	0.00097	998.7	954.0
51	1058.3	956.9	0.00652	0.00213	1058.9	962.3
52	991.3	956.8	-0.00465	0.00188	990.7	959.6
72	308.7	466.1	-0.11738	-0.07381	309.1	460.0
73	631.3	169.2	-0.06361	-0.12032	627.6	166.3
74	< 0.		0.00677	-0.16826		
75	1289.0	145.5	0.04345	-0.12472	1286.9	147.5
76	1599.7	512.8	0.09376	-0.06923	1601.9	511.1
77	1854.2	871.4	0.13368	-0.01343	1856.4	868.5
79	446.7	1305.6	-0.09686	0.06096	448.6	1313.2
80	658.1	1568.5	-0.06232	0.10267	660.4	1574.0
81	859.9	1062.3	-0.02618	0.01862	861.9	1062.1
82	901.0	752.9	-0.01855	-0.03039	903.6	753.8
83	1262.3	810.2	0.04038	-0.02179	1266.2	813.6
84	1147.8	1094.5	0.02102	0.02257	1149.6	1091.8
85	428.8	808.2	-0.09764	-0.02037	430.8	805.6
86	917.1	455.3	-0.01536	-0.07699	921.1	455.0
87	929.7	1349.0	-0.01562	0.06526	932.0	1352.8
88	1365.3	1510.5	0.05457	0.08908	1364.3	1505.4
89	1427.3	1158.7	0.06559	0.03205	1426.4	1153.9
90	1822.5	1179.6	0.12818	0.03670	1822.0	1184.1
91	571.9	482.3	-0.07281	-0.07230	573.7	477.7
92	1042.0	204.4	0.00429	-0.11599	1042.3	202.5
93	1247.6	464.3	0.03781	-0.07526	1249.4	470.5
94	1070.9	1733.6	0.00549	0.12544	1070.3	1721.4
95	546.9	1078.4	-0.07848	0.02291	549.8	1081.1

Table 4 Observed and predicted anchor positions on the image and the input angle of the incoming ray – uv grism clocked.

Observation number 74 was used partially. Although the anchor point could not be measured because it fell outside the detector, it was used to measure the scale factor for the Zemax model.

10.2.1 Accuracy of the anchor point for the uv clocked grism calibration

To determine the accuracy, the calibration file was first generated. Using the calibration file (`swwavcal20090609_v2_mss1_uc160_0.940.fits`), the anchor points were determined by bilinear interpolation in the calibration file. The distortion correction was much better than the uv nominal grism, due to the better positions from having lenticular filter images before and after the grism observation. As a result, the predicted anchor positions fall right on the spectrum. The only exceptions are from the observations with

Clocked uv Grism		
Spectrum ID (from Table 11)	Anchor wavelength error (Å)	Standard deviation of spectral lines used (1-sigma) wavelength error (Å)
34	29.7	12.5
35	-2.0	10.4
36	-61.7	21.0
37	9.8	10.4
51	2.4	8.2
52	26.0	25.6
72	33.5	8.7
73	13.4	13.7
75	1.9	5.6
76	11.6	9.9
77	-2.7	29.0
79	6.6	10.0
80	5.6	8.4
81	20.1	9.8
82	33.1	19.9
83	20.1	12.8
84	22.8	9.8
85	6.6	8.1
86	25.3	11.8
87	16.1	12.6
88	13.6	7.4
89	23.0	7.9
90	-23.5	26.8
91	24.5	11.1
92	25.5	8.1
93	13.1	5.5
94	35.1	24.8
95	28.2	16.0

Table 5 : Anchor and dispersion errors in the uv Clocked grism.

$XDET(\text{physical}) > 1500$, which for this calibration posed problems that will be addressed in the future. The data are given in Table 5, and Figure 20. The offset of the anchor normal to the dispersion was typically less than 4 pixels, and was not recorded.

10.2.2 Accuracy of the wavelengths using the uv clocked grism calibration file

As in the nominal grism, the wavelengths of spectral lines were measured in each calibration spectrum, and then compared with the predicted wavelength using the calibration file.

When the spectrum comes close to the edge of the detector, the discrepancy between observed and predicted wavelength grows. Following here, we will show some of the overall fits to the observed wavelengths to illustrate that.

The typical wavelength error is less than 15\AA , but at the end of the observed spectrum, the error can grow much larger. The best wavelength scale is for spectra closest to the centre (the boresight point, i.e., within about 400 pixels).

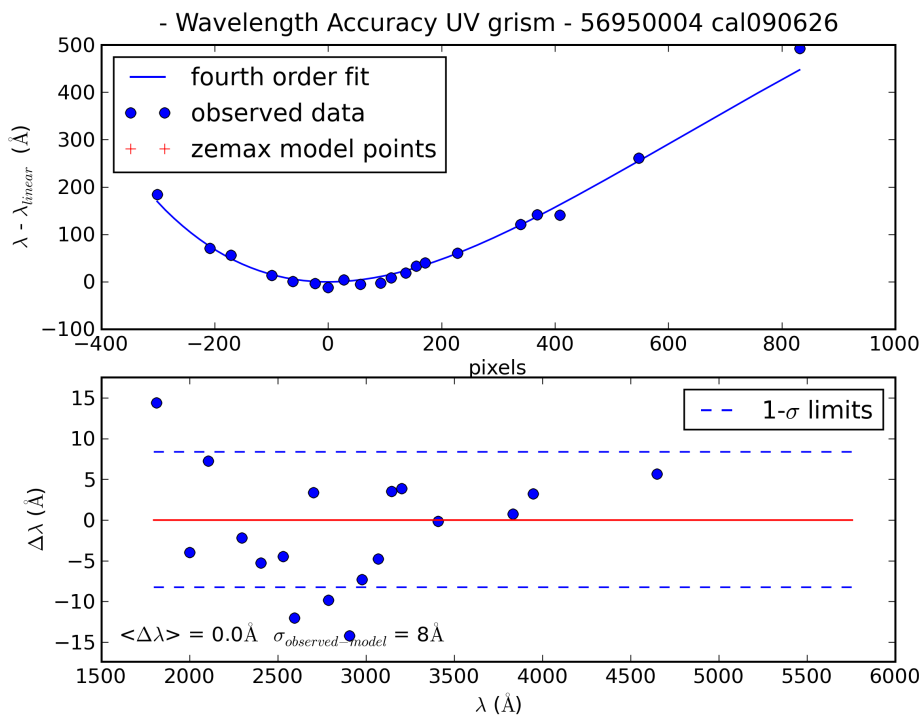


Figure 16. Wavelength accuracy for the uv clocked grism. Anchor for this spectrum is at $X, Y_{\text{phys}} = (547, 1078)$ on the left side of the detector image. For an explanation of the figure, see Figure 7.

In all these plots, and some of them have been cut short by the detector edge, the wavelengths deviate the most at the end of the range regardless of whether the end of the observed spectrum is at 1700 or 2000Å, 4000Å or 6000Å. This is probably due to some mismatch between the model, and the distortion correction or to the observation being too close to the edges of the detector, but at present we cannot be more specific as to the cause. Curiously, the same effect is not as apparent, or as large, in the nominal mode.

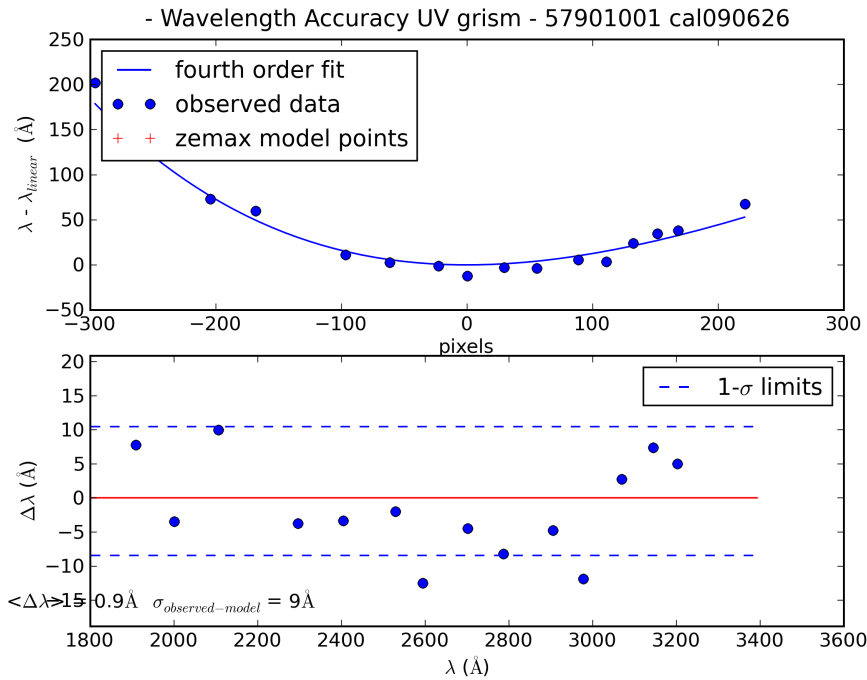


Figure 17. Wavelength accuracy for the uv clocked grism. Anchor at $X, Y_{\text{phys}} = (309, 466)$ in the bottom left corner of the detector image. For an explanation of the figure, see Figure 7.

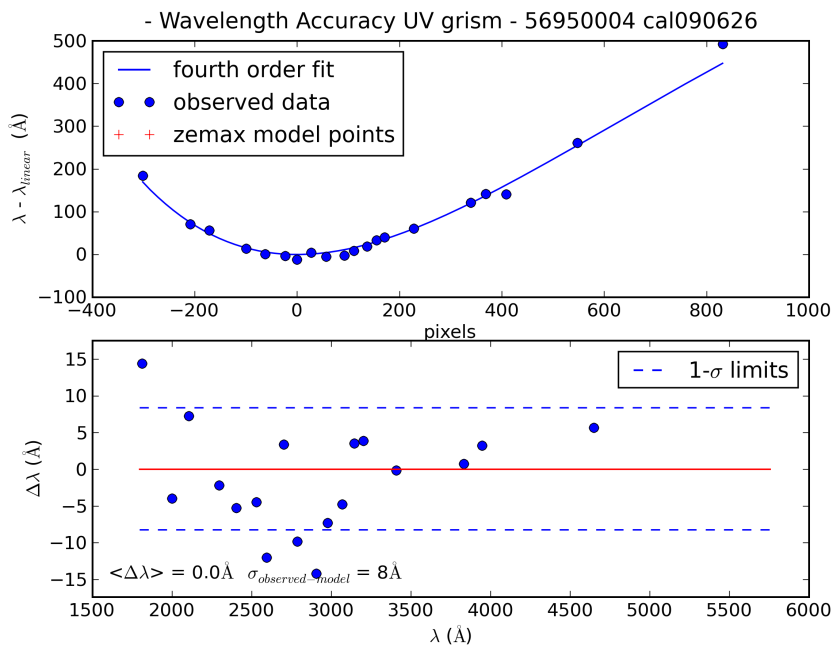


Figure 18. Wavelength accuracy for the uv clocked grism. Anchor at $X, Y_{\text{phys}} = (1000, 953)$, close to the boresight in the centre of the detector image. For an explanation of the figure, see Figure 7.

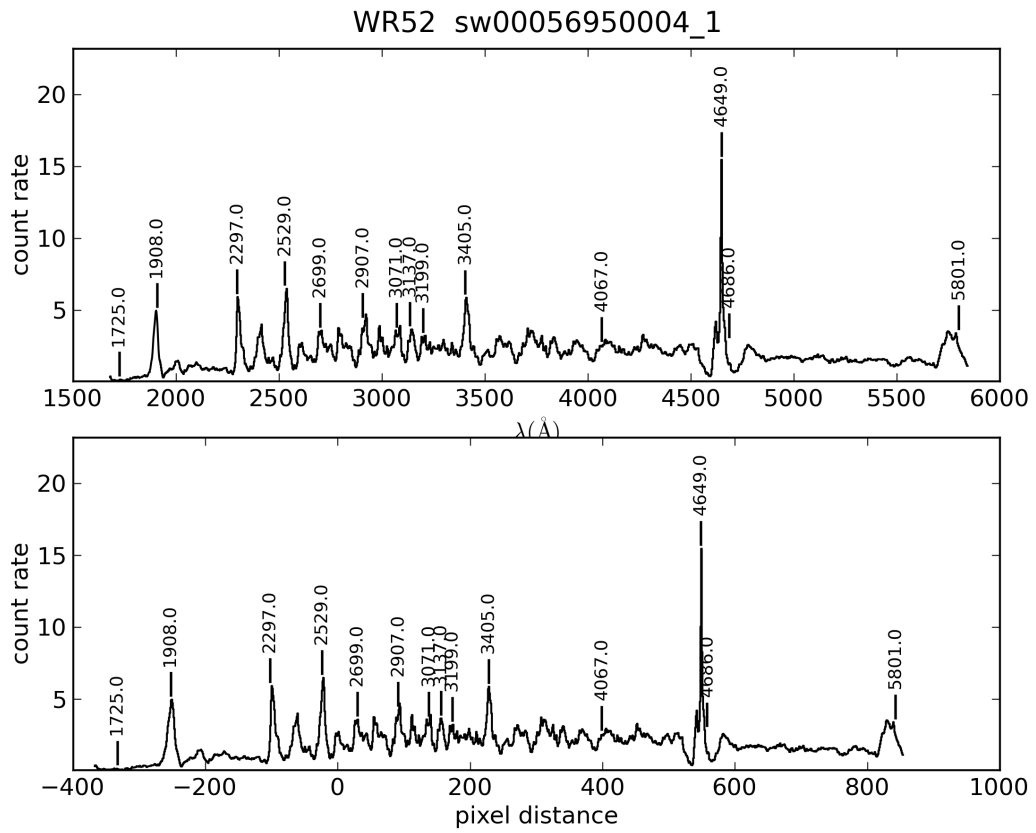


Figure 19. The spectrum corresponding to the accuracy analysis in Figure 18 with line identifications. The top panel is as function of wavelength, the lower panel as function of the distance in pixels to the anchor point.

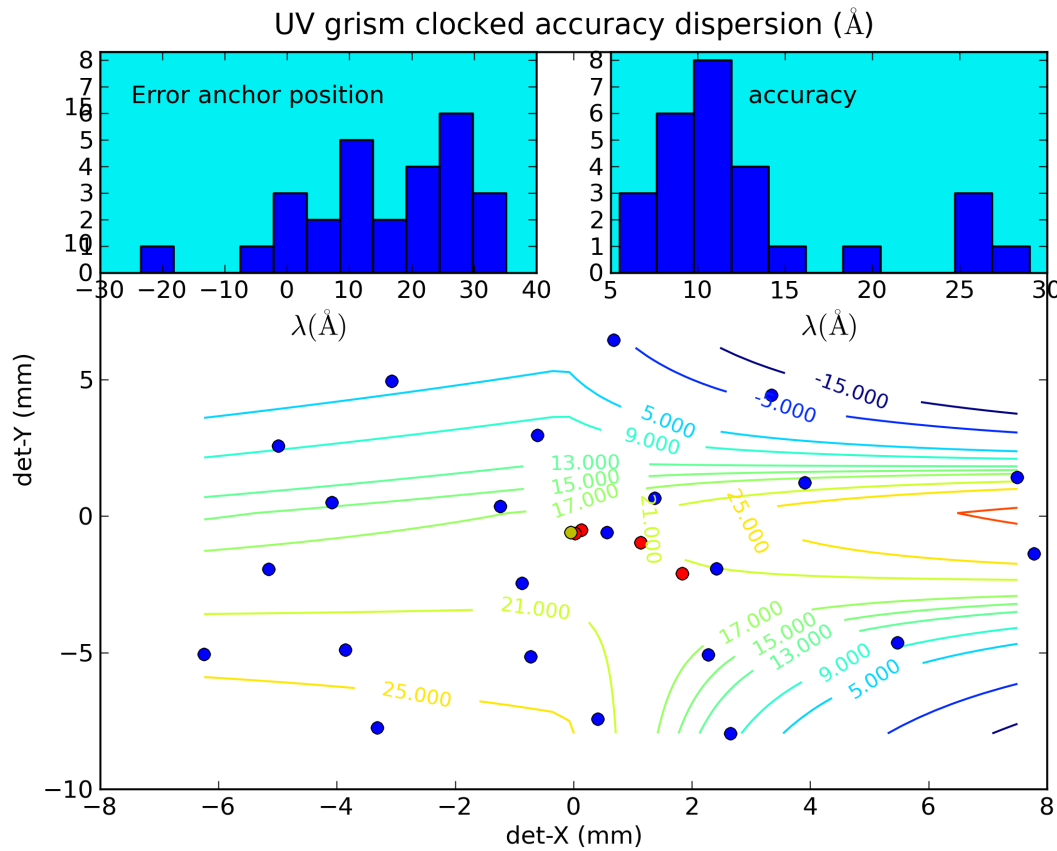


Figure 20. uv Clocked grism summary of wavelength error and accuracy. This figure shows the errors in the wavelength calibration. The blue dots are the anchor positions (at 260nm in first order) of the calibration spectra on the detector. The contours are a fit to the accuracy of the dispersion expressed as the RMS error between measured and predicted wavelength for known lines in the spectrum.

The inset in the top left corner shows that at most times the anchor point that was predicted using the source position in the lenticular filters taken just before and after the observation has a systematic offset of 15.9 Å. Disregarding the systematic offset, the anchor position typically falls within 23 Å (about 7 pixels) of the correct position. This is sufficient to avoid making misidentifications of the larger spectral features which have a FWHM which is comparable in magnitude.

The inset in the top right corner shows the accuracy of the adopted dispersion from the scaled zemax model after removal of the anchor point offsets as a root mean squared measure. The contours show the overall variation over the detector. For details, the actual fits given in the maps on this page should be consulted. The main result is, that the RMS error in the wavelengths in a spectrum is typically less than 16 Å, which is about 5 pixels.

10.3 V nominal grism

In the nominal V grism wavelength calibration the same methods were used as for the uv nominal grism discussed before in section 10.1. The calibration file used for the analysis of the errors was `swwavcal20100121_v0_mssl_vg1000.fits`. The observations used in this calibration have been listed in Table 14.

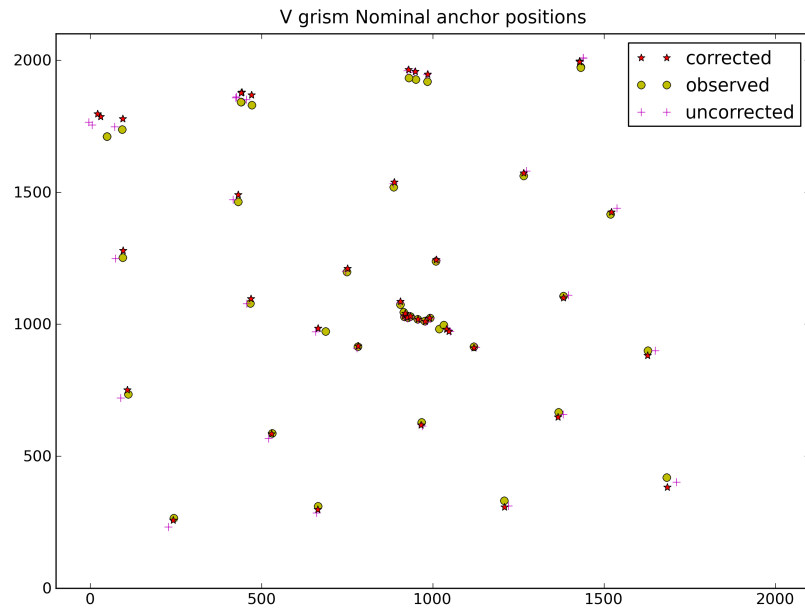


Figure 21. V Grism Nominal anchor positions. The observed as well as the Zemax model positions before and after applying the scaling correction (see section 8.4) shown are shown here.

Observed and predicted anchor positions on the image				
Spectrum ID	X _{obs}	Y _{obs}	X _{ank}	Y _{ank}
40	1018.4	981.5	1043.5	981.1
41	916.4	1028.7	916.1	1027.8
42	1032.0	997.2	1050.9	972.5
43	915.1	1045.2	919.3	1037.4
96	992.0	1023.1	992.6	1021.8
97	926.8	1024.6	925.3	1022.6
100	975.8	1011.6	979.3	1008.7
101	934.6	1029.4	934.6	1027.0
106	955.8	1018.6	957.5	1016.3
107	687.2	973.2	657.8	971.8
110	904.7	1074.6	904.0	1081.7
112	48.9	1710.8	4.95	1754.3
113	48.8	1710.9	-4.5	1764.9
118	440.3	1841.4	425.9	1860.7
119	439.3	1841.4	424.3	1858.0
120	111.0	735.2	88.8	720.8
122	243.3	265.1	228.0	231.8
124	950.5	1927.4	945.1	1954.9
125	929.8	1933.3	925.4	1961.1
126	1431.5	1974.4	1439.1	2009.2
127	1431.5	1972.4	1439.1	2007.3
128	1518.4	1416.1	1537.5	1439.9
129	1627.7	900.3	1649.2	900.1
130	1682.8	419.7	1711.0	401.8
132	1208.1	332.0	1220.6	311.4
133	665.0	310.3	660.4	285.8
134	1367.2	666.6	1380.3	658.0
135	967.5	628.8	968.7	614.7
136	530.8	586.5	520.7	567.6
137	467.3	1079.0	456.5	1078.2
138	431.8	1463.6	416.9	1471.2
139	885.3	1519.6	884.4	1533.1
140	1265.3	1562.2	1272.7	1580.3
141	95.1	1252.1	73.7	1249.4
142	1381.2	1107.3	1395.0	1110.2
143	1119.9	914.5	1125.8	912.5
162	780.8	914.8	778.7	908.7
163	749.0	1197.7	745.5	1201.4
164	1009.1	1238.0	1011.5	1243.2
167	93.4	1737.1	71.1	1748.4
168	471.2	1830.4	455.6	1850.5
169	983.8	1919.1	982.7	1945.6

Table 6 : V Grism Nominal anchor positions.

10.3.1 Accuracy of the anchor point for the V nominal grism calibration

Nominal V Grism		
Spectrum ID (from Table 13)	Anchor wavelength error (Å)	Standard deviation of spectral lines used (1-sigma) wavelength error (Å)
107	-7.6	14.6
110	-26.0	6.8
118	12.2	6.1
119	9.3	11.1
120	-15.3	4.1
124	1.3	6.1
125	7.1	3.1
129	-13.3	5.0
130	13.7	7.7
132	-2.2	5.7
133	-4.0	5.6
134	-4.6	6.1
135	1.6	4.9
136	-4.7	3.7
137	4.9	5.4
138	6.3	4.2
139	14.8	8.9
140	-1.7	7.2
141	3.7	5.6
142	3.3	5.1
143	-5.7	3.2
162	-3.4	5.2
163	10.6	5.8
164	-2.1	4.4
167	8.0	11.1
168	-6.9	6.1
169	21.9	7.4

Table 7 : V grism Nominal Anchor error

10.3.2 Accuracy of the wavelengths using the V nominal grism calibration file

The following figures show the accuracy of the wavelengths using the calibration file following the same procedure as in the UV Nominal Grism in section 10.1. The main difference is that the V grism dispersion can be well fitted by a third order polynomial, and the curvature of the spectrum has been negligible.

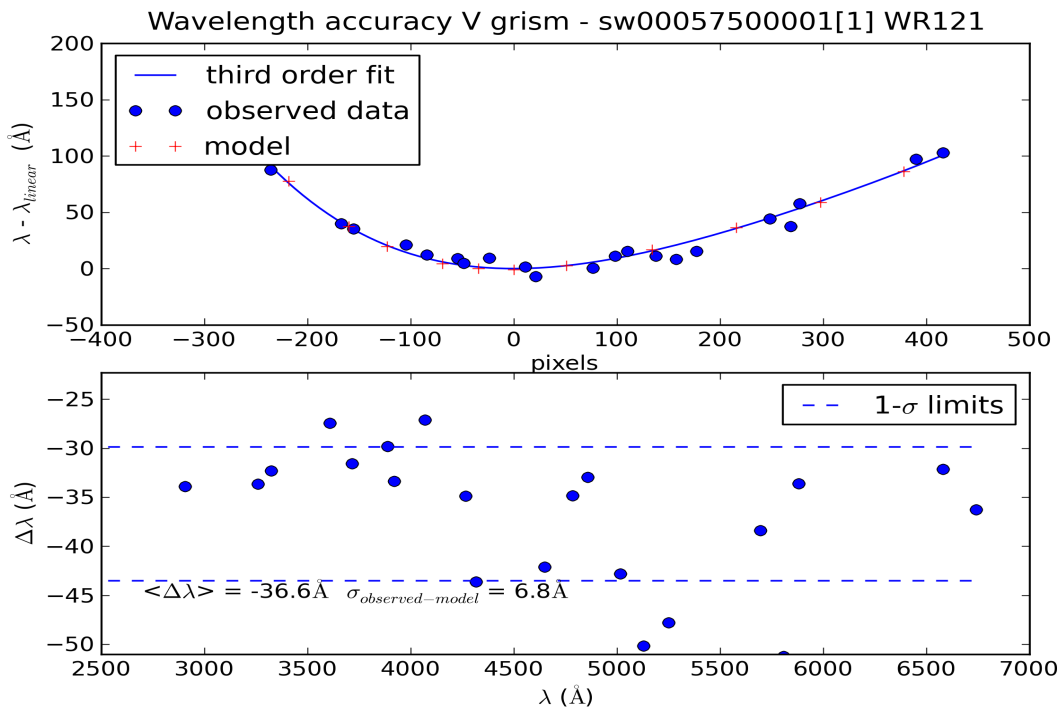


Figure 22. Wavelength accuracy for the V clocked grism (spectrum ID=110). Anchor at $X, Y_{\text{phys}} = (904, 1081)$ which is in the middle of the detector image. For an explanation of the figure, see Figure 7.

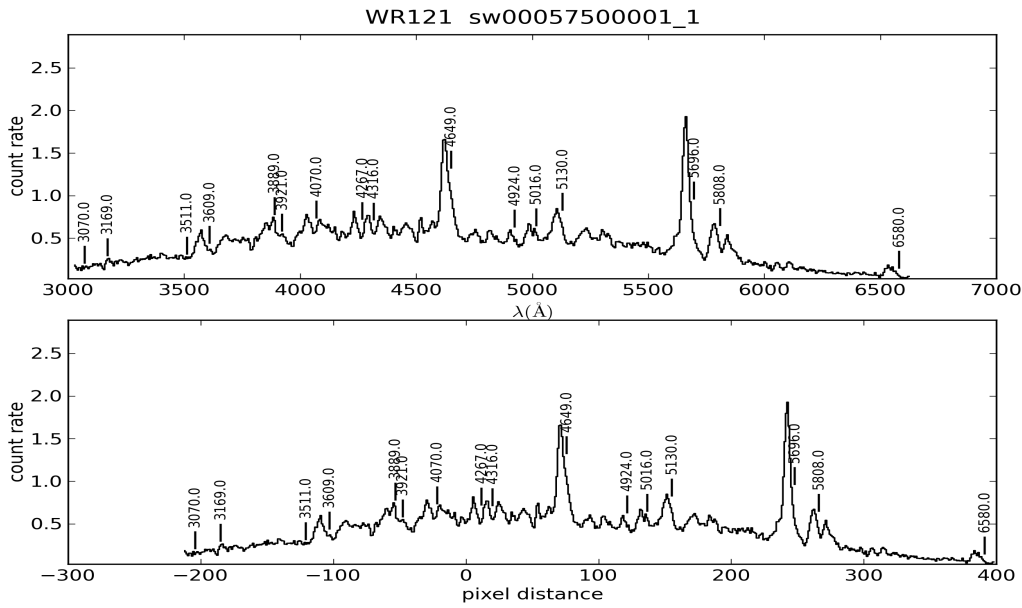


Figure 23. Spectrum with line identifications used to generate the accuracy plot Figure 22. Notice the anchor offset causes the line ID's to misalign with the spectral features, and compare to the accuracy plot.

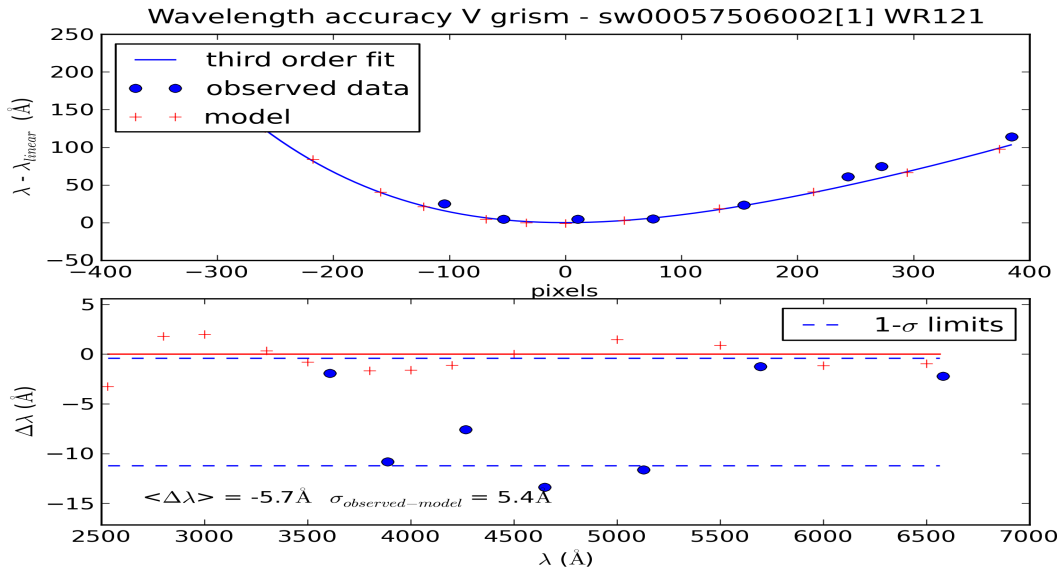


Figure 24. Wavelength accuracy for the V clocked grism (spectrum ID=137). Anchor at $X, Y_{\text{phys}} = (457, 1078)$ which is on the left side of the detector image. For an explanation of the figure, see Figure 7

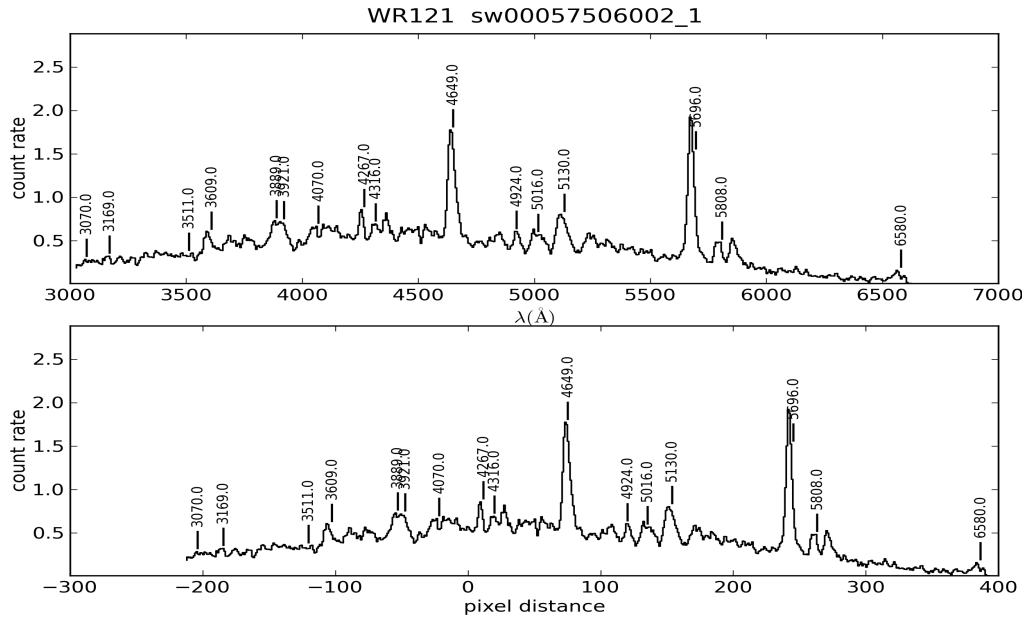


Figure 25. Spectrum with line identifications used to generate the accuracy plot Figure 24.

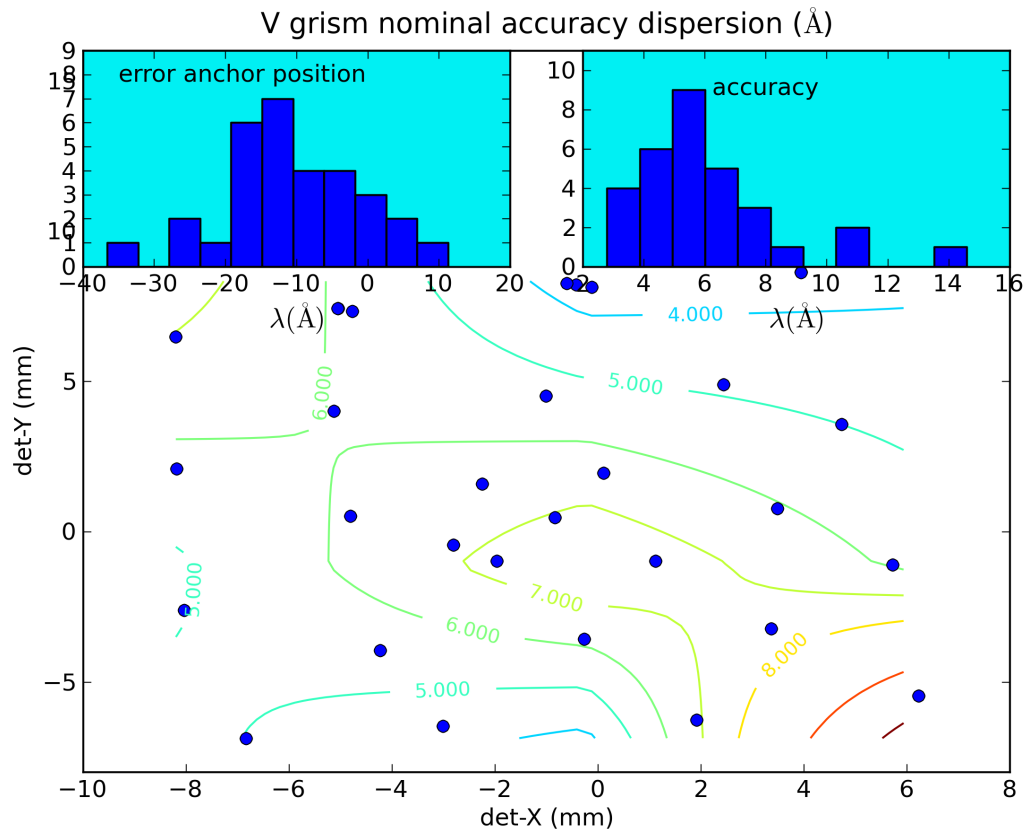


Figure 26. Summary of the accuracy of the V Nominal grism. This figure shows the errors in the wavelength calibration. The small inset in the top left corner shows that at most times the anchor point that was predicted using the lenticular filters taken just before and after the observation, falls within 20 Å (about 4 pixels) of the correct position. The contours provide more details on how the remaining anchor offsets typically vary across the detector. This is usually sufficient to avoid making misidentifications of the larger spectral features which have a FWHM which is comparable in magnitude. The right inset shows the accuracy of the adopted dispersion from the scaled zemax model after removal of the anchor point offsets as a root mean squared measure. For details, the actual fits given in the figures accessible from the maps on this page should be consulted. The main result is, that the RMS error in the wavelengths in a spectrum is typically less than 11 Å, which is about 2 pixels.

The wavelength accuracy represents a mix of the goodness of the fit of the scaled Zemax model dispersion and the ability to measure line positions well enough in the spectra. It should be expected that any spectrum using this calibration will have comparable uncertainties in the wavelength determination. A final caveat is that the calibration observations were mostly made using an observing mode with both a lenticular filter observation before and after the grism exposure, like uvw1+grism+uvw1. Any position changes of the source seen in the lenticular images were dealt with by taking the middle of the position before and after the grism exposure. Typically the differences were less

than 3 pixels, but exceptions with larger drifts have been seen. Details on the fits of the individual calibration observations can give an indication on how well the calibration can be trusted and also, what to expect for an observation away from the centre of the detector. The complete set of spectra used for the calibration can be found on-line^x.

10.4 V clocked grism

The same methods were used as for the uv nominal grism, see section 10.1. The calibration file used for the error analysis was `swwavcal20100421_v0_mssl_vc955_wlshift-8.0.fits`. The observations used can be found in Table 13.

Observed and predicted anchor positions on the image				
Spectrum ID	X_{obs}	Y_{obs}	X_{ank}	Y_{ank}
38	1153.6	956.5	1142.7	954.1
39	1041.6	954.5	1046.2	953.9
46	1148.5	898.5	1143.1	923.2
98	1094.6	951.5	1095.7	951.4
99	1056.6	955.5	1059.2	950.3
102	1104.6	957.5	1107.6	958.9
103	1046.6	959.5	1047.3	954.4
105	1088.6	944.5	1090.4	939.5
108	767.6	814.5	765.8	814.5
131	802.0	977.7	802.5	980.9
121	269.4	652.2	267.3	652.8
123	382.8	183.7	383.5	185.3
146	1114.4	1801.0	1113.5	1804.1
147	1766.8	850.2	1765.0	853.3
148	1798.6	385.5	1799.4	384.7
149	1310.4	305.8	1309.4	306.3
150	802.8	225.2	803.1	224.4
151	1453.6	604.9	1452.9	604.3
152	1053.9	576.2	1055.3	575.6
153	675.8	500.6	676.4	497.3
154	593.4	1004.0	593.9	1006.2
155	568.7	1377.1	568.2	1378.3
156	993.8	1436.5	995.5	1431.8
157	1330.3	1475.1	1330.5	1473.0
158	1431.9	1050.1	1434.6	1049.5
159	934.5	847.6	935.3	844.6
160	879.5	1153.1	879.7	1151.1
161	1147.4	1179.3	1147.9	1175.5

^x <http://www.mssl.ucl.ac.uk/~npmk/Grism>

165	1579.5	1894.6	1578.6	1896.9
166	1703.7	1427.9	1704.8	1424.8

Table 8 : V clocked grism anchor positions

10.4.1 Accuracy of the anchor point for the V clocked grism calibration

The using the fits to the spectral lines the errors in the following table were found.

Clock V Grism		
Spectrum ID (Table 13)	Anchor wavelength error (Å)	Standard deviation of spectral lines used (1-sigma) wavelength error (Å)
108	-10.9	6.2
131	-12.3	8.0
121	-21.3	26.9
123	-4.9	10.3
146	-2.6	6.1
147	-20.9	8.5
148	-7.7	6.5
149	-10.9	8.1
150	-3.9	6.7
151	-13.2	10.6
152	0.8	5.0
153	1.6	5.4
154	-9.4	15.6
155	12.0	15.5
156	17.5	8.7
157	4.5	9.2
158	4.0	12.3
159	-1.5	6.1
160	11.2	6.8
161	13.0	6.9
166	0.8	14.2

Table 9 : Anchor and dispersion errors in the V Clocked grism

10.4.2 Accuracy of the wavelengths using the V clocked grism calibration file

Wavelength accuracy plots were made for each useful calibration spectrum. The format of the accuracy plots is to have two panels. Since the main variation of the dispersion can be represented by a constant with a linear term, the top panel of the accuracy plot has taken those two terms out. The higher order terms tend to zero near the adopted anchor point, which for the V-clocked grism mode is $\sim 4200\text{\AA}$. The dispersion from the scaled

optical model has been approximated with a polynomial. The observed line positions from lines identified in the calibration spectrum have been plotted as blue dots. The lower panel of these wavelength accuracy plots shows the remainder after subtraction of the predicted position. The observed position was found from the pixel distance to the anchor point and the dispersion relation, while the predicted position was found using the known wavelength. If the model dispersion is good, the difference can be divided into an offset and a random looking spread around that offset. The values for that case are given in the plot. In some points near the edges of the detector, the scaled model dispersion deviates and the points will not evenly be distributed around some mean offset.

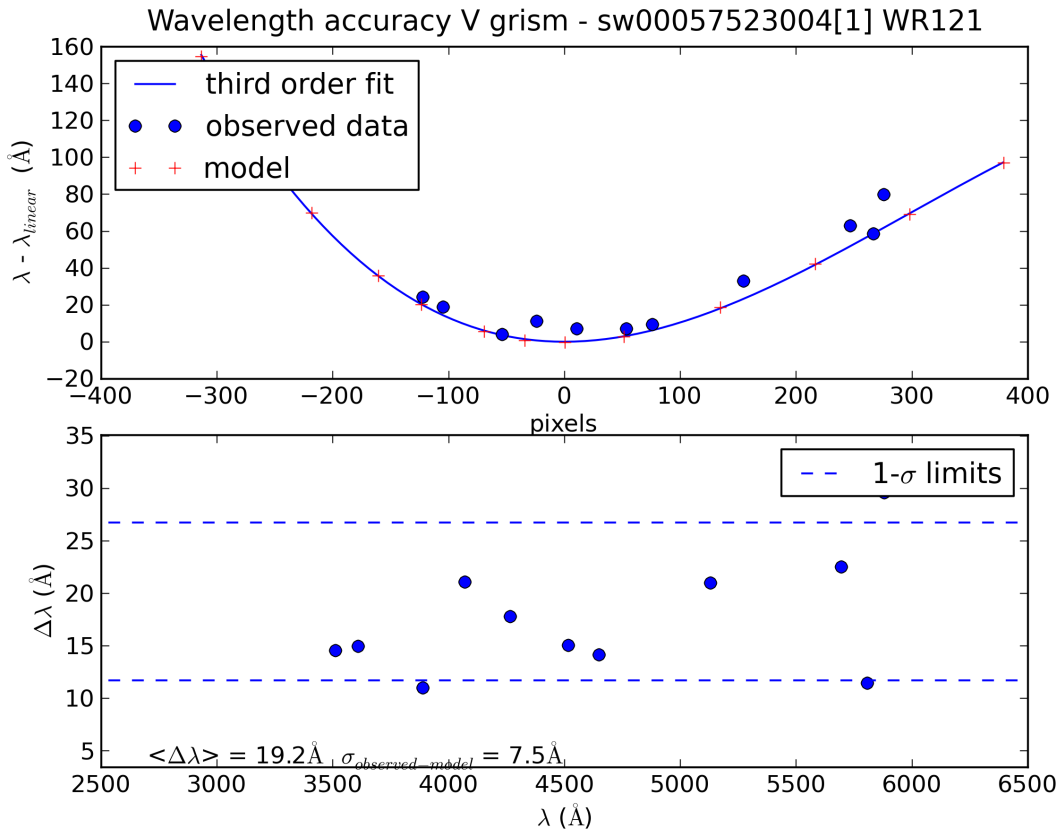


Figure 27. Wavelength accuracy for the V clocked grism (spectrum ID=147). Anchor at $X, Y_{\text{phys}} = (1765, 853)$ which is on the right hand side of the detector image. For an explanation of the figure, see Figure 7.

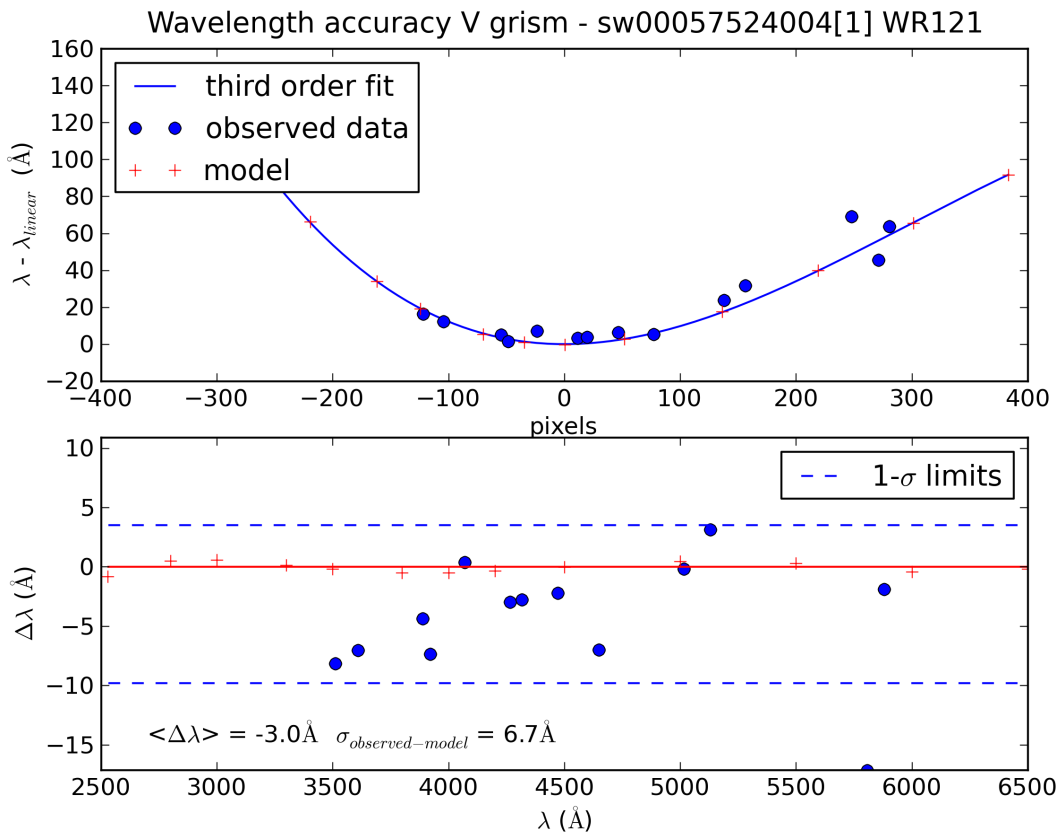


Figure 28. Wavelength accuracy for the V clocked grism (spectrum ID=148). Anchor at $X, Y_{\text{phys}} = (1799, 385)$ which is on the bottom right of the detector image. For an explanation of the figure, see Figure 7.

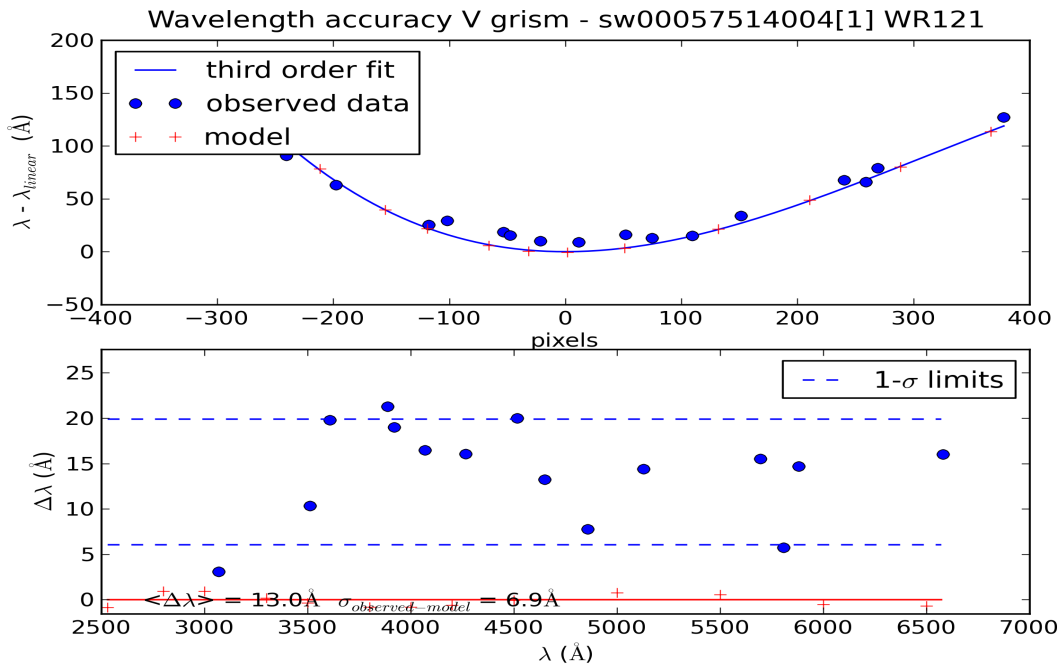


Figure 29. Wavelength accuracy for the V clocked grism (spectrum ID=161). Anchor at $X, Y_{\text{phys}} = (1148, 1175)$ which is in the middle of the detector image. For an explanation of the figure, see Figure 7.

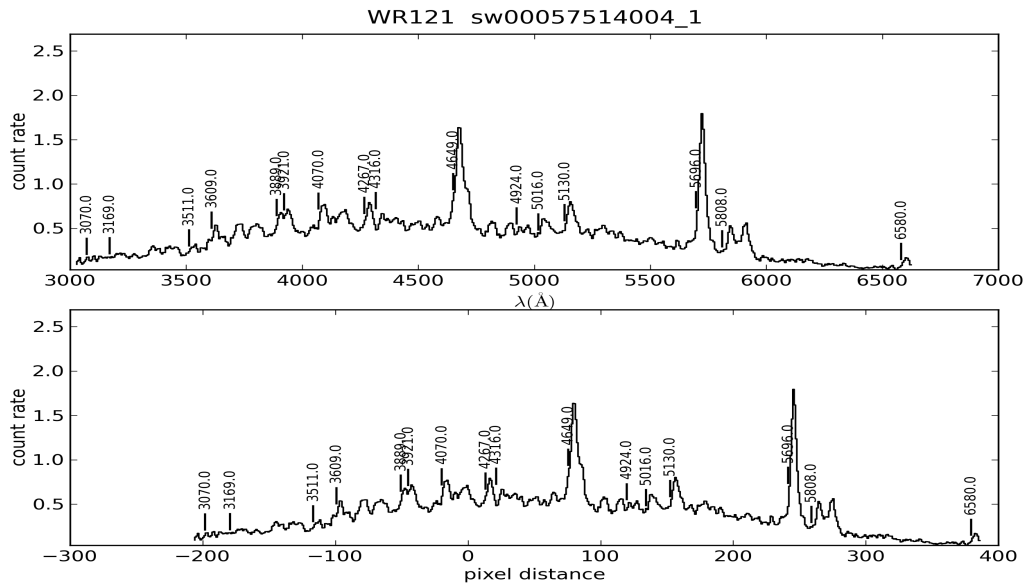


Figure 30. Spectrum with line identifications used to generate the accuracy plot Figure 29. Notice the anchor offset causes the line ID's to misalign with the spectral features, and compare to the accuracy plot.

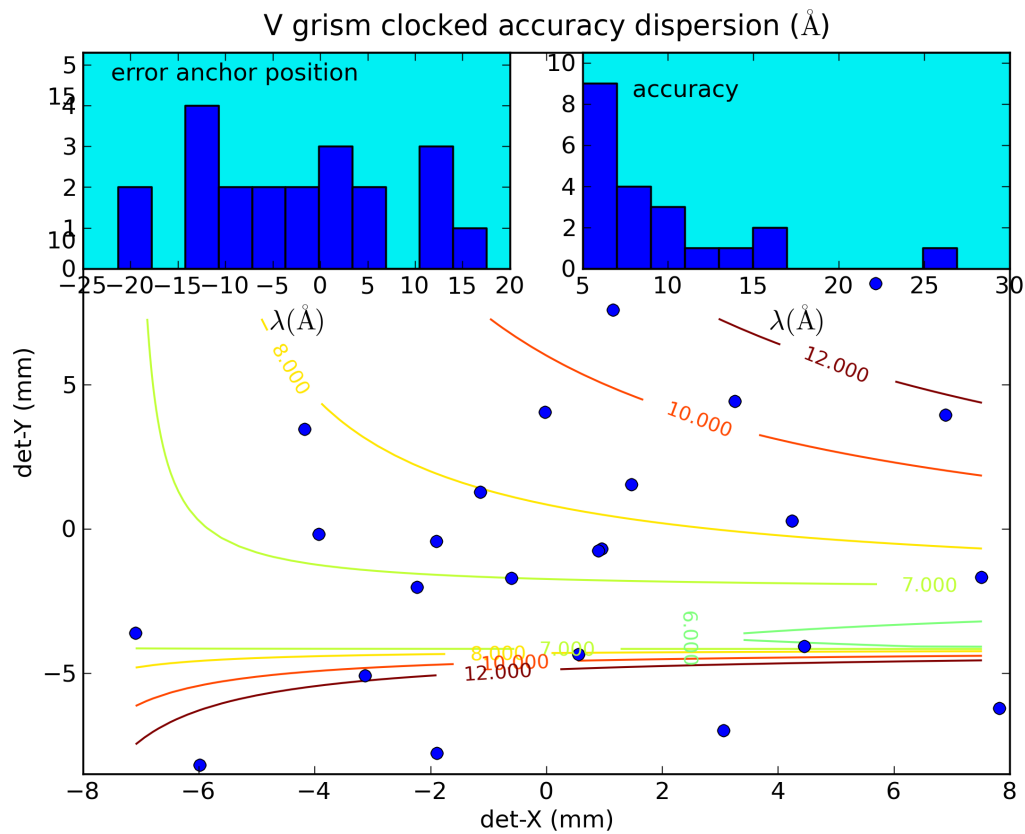


Figure 31. Summary of the wavelength accuracy for the V clocked grism. This figure shows the errors in the wavelength calibration. The small inset in the top left corner shows that at most times the anchor point that was predicted using the lenticular filters taken just before and after the observation, falls within 22 Å (about 3 pixels) of the correct position. This is sufficient to avoid making misidentifications of the larger spectral features which have a FWHM which is comparable in magnitude. The right inset and the main figure show the accuracy of the adopted dispersion as a root mean squared measure for the scaled zemax model after removal of the anchor point offsets. The main result is, that the RMS error in the wavelengths in a spectrum is typically less than 17 Å, which is about 3 pixels.

The upper left corner (low det-X , high det-Y) has no first orders because of the aperture cuts off illumination which is due to rotating the filterwheel.

11 Discussion and Summary

The table below lists the range within which most of the calibration spectra fall. The numbers in our analysis are too low to be able to say whether the distribution looks like a normal distribution, so the RMS error may not be appropriate. Most of the spectra will have a wavelength within the specified ranges.

Grism Mode	Anchor accuracy range in Å	Dispersion Error Å
uv Nominal	33	14
uv Clocked	23	16
V Clocked	22	17
V Nominal	20	11

Table 10 : Summary of wavelength accuracy of the new calibration for whole detector.

In practice, many older observations exist that do not have an accompanying lenticular filter taken during the same observing sequence. Even in the future that may not always be possible if a bright source is in the field. In those cases the input angle (see the beginning of section 7) must be determined using the grism image itself. The aspect needs to be corrected using `uvotgraspccorr`, and the attitude correction needs to be used to determine the input angle correctly. The wavelength error component due to an error in the anchor position (a shift in the wavelength scale) then is proportional to the error in the aspect correction.

The present calibration applies at each anchor position a simple scaling factor to the dispersion from the Zemax model. However, the model does not have the proper diffraction constants for the uv grism below 1900Å, and the use of the peak of the PSF from the model may skew the dispersion at long wavelengths due to the asymmetric and extended PSF. There seems to be some systematic increase in the dispersion error, as can be seen from the wavelength accuracy plots, so there is some room for improvement.

There is some degradation in performance in the current calibration of the clocked uv mode when the anchor point is located within 300 pixels of the right hand side of the detector (large DETX). A similar effect has not been seen the nominal mode calibration, but within 50 pixels of the rhs detector edge the predicted dispersion changes a lot. This will be investigated in the future. Fortunately, few pointed spectra are in that region.

The rotation of the image before extraction implies a resampling of the data over neighboring pixels. The grism point spread function in the uv grism varies from about 2.9Å in the blue part of the spectrum to very broad in the red part. That means that the PSF broadening is of the size of a pixel or larger. In addition broadening due to pointing jitter of the spacecraft exists, which is also of the order of a pixel. Resampling does therefore only add a relatively small extra broadening to the blue part of the spectrum.

The overall consistency provided by the optical model gives a common benchmark against which all these observations have been tested, and provides an understanding of the variation over the detector of that uncertainty. We think that the current wavelength calibration is good enough to be used over the whole detector to yield wavelengths accurate within the stated uncertainties.

The final wavelength calibration files (with final corrections as mentioned) are:

swugu0160wcal20041120v001.fits,
swugu0200wcal20041120v001.fits,
swugv0955wcal20041120v001.fits,
swugv1000wcal20041120v001.fits.

12 References

Breeveld et al., 2010, Monthly Notices of the Royal Astronomical Society, Volume 406, pp 1687-1700.

Poole et al., 2008. Monthly Notices of the Royal Astronomical Society, Volume 383, Issue 2, pp. 627-645.

Roming et al. 2004. GAMMA-RAY BURSTS: 30 YEARS OF DISCOVERY: Gamma-Ray Burst Symposium. AIP Conference Proceedings, Volume 727, pp. 651-654.

Teldef file documentation, SWIFT UVOT CALDB RELEASE NOTE.

http://heasarc.gsfc.nasa.gov/docs/heasarc/caldb/swift/docs/uvot/uvot_caldb_teldef_01.pdf

13 Larger Tables

UVOT observations of sources used for the nominal uv grism calibration						
ID	Object	OBSID	EXT	Grism image	Lenticular Filter Image	Date
1	WR52	56950007	1	gu231139384I	w1231394014I	080502
2	WR86	57000005	1	gu231383283I	w1231383514I	080502
3	WR52	56950007	2	gu231399443I	w1231399744I	080502
4	WR86	57000005	2	gu231388883I	w1231389214I	080502
5	WR1	37905003	1	gu238539623I	w1238540074I	080723
6	WR86	57011002	1	gu236456305I	w1236456305I	080629
7	WR86	57012002	1	gu236462064I	w1236462424I	080629
8	WR86	57013002	1	gu236543063I	w1236543424I	080629
9	WR86	57014002	1	gu236548824I	w1236549185I	080630
10	WR86	57018001	1	gu242197488I	w1242197979I	080904
11	WR86	57018002	1	gu242198243I	W1242198694I	080904
12	WR86	57015001	1	gu242208781I	W1242209111I	080904
13	WR86	57015002	1	gu242209403I	W1242209793I	080904
14	WR86	57016001	1	gu242214541I	W1242214932I	080904
15	WR86	57016002	1	gu242215284I	W1242215614I	080904
16	WR86	57017001	1	gu242220361I	W1242220692I	080904
17	WR86	57017002	1	gu242220983I	W1242221375I	080904

UVOT observations of sources used for the nominal uv grism calibration						
ID	Object	OBSID	EXT	Grism image	Lenticular Filter Image	Date
18	WR86	57019001	1	gu244152311I	W1244152640I	080926
19	WR86	57019002	1	gu244152983I	W1244153285I	080926
20	WR86	57020001	1	GU244158133I	W1244158463I	080926
21	WR86	57020002	1	GU244158743I	W1244159074I	080926
22	WR86	57021001	1	GU244163953I	W1244164284I	080926
23	WR86	57021002	1	GU244164564I	W1244164864I	080926
24	WR86	57022001	1	GU244169713I	W1244170043I	080927
25	WR86	57022002	1	GU244170324I	W1244170655I	080927
26	WR86	57023001	1	GU244175414I	W1244175745I	080927
27	WR86	57023002	1	GU244176024I	W1244176505I	080927
28	WR86	57024001	1	gu244238954I	w1244239285I	080927
29	WR86	57024002	1	gu244239564I	w1244239863I	080927
30	WR86	57025001	1	gu244244953I	w1244245283I	080927
31	WR86	57025002	1	gu244245563I	w1244245864I	080927
32	WR86	57026001	1	gu244250533I	w1244250864I	080927
33	WR86	57026002	1	gu244251144I	w1244251443I	080927

Table 11 : uv Nominal observations used

UVOT observations of sources used for the clocked uv grism calibration							
ID	Object	OBSID	E X T	Lenticular Filter Image	Grism image	Lenticular Filter Image	Date
34	WR4	56900001	1		gu248231372I	w1248231822I	081113
35	WR4	56900002	1		gu248232264I	w1248232685I	081113
36	WR4	56900003	1		gu250065349I	w1250065300I	081204
37	WR4	56900004	1		gu250065853I	w1250065803I	081204
51	WR52	56950004	1		gu230531544I	w2230532302I	080422
52	WR86	57000002	1		gu230487624I	w2230488109I	080421
72	WR52	57901001	1	w1256729765E	gu256729814I	w1256730256E	090219
73	WR52	57902001	1	w1256734981E	gu256735030I	w1256735472E	090219
74	WR52	57903001	1	w1256735524E	gu256735573I	w1256736015E	090219
75	WR52	57904001	1	w1256740741E	gu256740791I	w1256741233E	090219
76	WR52	57905001	1	w1256741284E	gu256741333I	w1256741775E	090219
77	WR52	57906001	1	w1256741824E	gu256741875I	w1256742317E	090219
79	WR52	57908001	1	w1256746510E	gu256746559I	w1256747001E	090219
80	WR52	57909001	1	w1256752270E	gu256752319I	w1256752760E	090219
81	WR52	57911001	1	w1256747044E	gu256747093I	w1256747535E	090219
82	WR52	57912001	1	w1256747585E	gu256747634I	w1256748076E	090219
83	WR52	57913001	1	w1256748124E	gu256748173I	w1256748615E	090219
84	WR52	57914001	1	w1256752805E	gu256752854I	w1256753297E	090219
85	WR52	57915001	1	w1256753344E	gu256753393I	w1256753835E	090219

UVOT observations of sources used for the clocked uv grism calibration							
ID	Object	OBSID	E X T	Lenticular Filter Image	Grism image	Lenticular Filter Image	Date
86	WR52	57916001	1	w1256753884E	gu256753933I	w1256754375E	090219
87	WR52	57918001	1	w1256759135E	gu256759184I		090219
88	WR52	57919001	1	w1256759644E	gu256759694I	w1256760135E	090219
89	WR52	57920001	1	w1256764385E	gu256764434I	w1256764876E	090220
90	WR52	57921001	1	w1256763844E	gu256763893I	w1256764335E	090220
91	WR52	57922001	1	w1256764924E	gu256764973I	w1256765415E	090220
92	WR52	57923001	1	w1256765464E	gu256765515I	w1256765956E	090220
93	WR52	57924001	1	w1256769603E	gu256769652I	w1256770095E	090220
94	WR52	57925001	1	w1256770145E	gu256770200I	w1256770691E	090220
95	WR52	57926001	1	w1256776767E	gu256776821I	w1256777314E	090220

Table 12 : uv clocked observations used

UVOT observations of sources used for the clocked V grism calibration							
ID	Object	OBSID	E X T	Lenticular Filter Image	Grism image	Lenticular Filter Image	Date
99	WR52	56950014	1	w1273315863E	gv273315909I	w1273316299E	090831
102	WR52	56950019	1	w1273367344E	gv273367390I	w1273367780E	090831
103	WR52	56950020	1	w1273367823E	gv273367870I	w1273368259E	090831
105	WR92	37906005	1	w1274440643E	gv274420700I	w1274421190I	090912
108	WR81	57550002	1	W1275824786E	Gv275824878I	W1275825719E	090928
131	WR121	57500002	1	W1275906485E	Gv275824878I	W1275907417E	090929
114	WR121	57502002	1	w1278641944E	gv278642050I	w1278643041E	091031
115	WR121	57502002	2	w1278647884E	gv278647940I	w1278648430E	091031
116	WR121	57502004	1	w1278671163E	gv278671256I	w1278672096E	091031
117	WR121	57502004	2	w1278682923E	gv278683000I	w1278683690E	091031
121	WR121	57504004	1	w1278578104E	gv278578246I	w1278579588E	091030
123	WR121	57507004	1	w1278503344E	gv278503500I		091029
144	WR121	57501004	1	w1279491665E	gv279491821I	w1279493314E	091109
145	WR121	57503004	1	w1279497624E	gv279497780I		091109
146	WR121	57508004	1	w1279514985E	gv279515142I		091110
147	WR121	57523004	1	w1279532464E	gv279532620I	w1279534112E	091110
148	WR121	57524004	1	w1279538164E	gv279538320I	w1279539812E	091110
149	WR121	57521004	1	w1279544224E	gv279544380I	w1279545873E	091110
150	WR121	57513004	1	w1279595763E	gv279595919I	w1279597411E	091110
151	WR121	57522004	1	w1279601584E	gv279601740I	w1279603232E	091110
152	WR121	57516004	1	w1279607764E	gv279607922I	w1279609414E	091111
153	WR121	57511004	1	w1279613103E	gv279613260I	w1279614752E	091111
154	WR121	57506004	1	w1279624864E	gv279625020I	w1279626513E	091111
155	WR121	57505004	1	w1279630865E	gv279631021I	w1279632513E	091111
156	WR121	57509004	1	w1279659424E	gv279659581I		091111

UVOT observations of sources used for the clocked V grism calibration							
ID	Object	OBSID	E X T	Lenticular Filter Image	Grism image	Lenticular Filter Image	Date
157	WR121	57515004	1	w1279677003E	gv279677161I	w1279678653E	091112
158	WR121	57519004	1	w1279693984E	gv279694140I	w1279695632E	091112
159	WR121	57512004	1	w1279705625E	gv279705781I	w1279707273E	091112
160	WR121	57510004	1	w1279711624E	gv279711780I	w1279713271E	091112
161	WR121	57514004	1	w1279717504E	gv279717660I	w1279719152E	091112
165	WR121	57518006	1	w1279763526E	gv279763682I	w1279765174E	091113
166	WR121	57520006	1	w1279769224E	gv279769380	w1279770872E	091113

Table 13 : V clocked grism observations used

UVOT observations of sources used for the nominal V grism calibration							
ID	Object	OBSID	EXT	Lenticular Filter Image	Grism image	Lenticular Filter Image	Date
40	WR4	56900007	1		gv250071120I	w1250071509I	081204
41	WR4	56900008	1		gv250071863I	w1250072253I	081204
42	HD5980	57250001	1		gv249226141I	gv249226141I	081124
43	HD5980	57250002	1		gv249227003I	w1249227451I	081124
96	WR52	56950010	1	w1273309563E	gv273309610I	w1273309999E	090830
97	WR52	56950011	1	w1273310044E	gv273310090I	w1273310480E	090830
100	WR52	56950016	1	w1273332725E	gv273332771I	w1273333160E	090831
101	WR52	56950017	1	w1273333204E	gv273333250I	w1273333639E	090831
106	WR92	37906003	1	w1274374743E	gv274374805I	w1274375345E	090911
107	WR81	57550001	1	w1275813095E	GV275813191I	w1275813095E	090928
110	WR121	57500001	1	w1275895503E	gv275895595I	w1275896435	090929
112	WR121	57501002	1	w1278734224E	gv278734312I	w1278735103E	091101
113	WR121	57501002	2	w1278739985	gv278740062I	w1278740753	091101
118	WR121	57503002	1	w1278745804E	gv278745891I	w1278746681	091101
119	WR121	57503002	2	w1278751564E	gv278751640I	w1278752330E	091101
120	WR121	57504002	1	w1278572283E	gv278572430I	w1278573822E	091030
122	WR121	57507002	1	w1278497104E	gv278497261I		091029
124	WR121	57508002	1	w1278815164E	gv278815257I	w1278816098E	091102
125	WR121	57508002	2	w1278820983E	gv278821076I	w1278821918E	091102
126	WR121	57518002	1	w1278826923E	gv278827014I		091102
127	WR121	57518002	2	w1278832684E	gv278832776I		091102
128	WR121	57520002	1	w1278907931E	gv278908087I		091103
129	WR121	57523002	1	w1278982744E	gv278982895I	w1278984337E	091103
130	WR121	57524002	1	w1279012263E	gv279012419I	w1279013912E	091104
132	WR121	57521002	1	w1279254665E	gv279254821I	w1279256313E	091107
133	WR121	57513002	1	w1279260424E	gv279260582I	w1279262073E	091107
134	WR121	57522002	1	w1279266184E	gv279266340I	w1279267833E	091107

UVOT observations of sources used for the nominal V grism calibration							
ID	Object	OBSID	EXT	Lenticular Filter Image	Grism image	Lenticular Filter Image	Date
135	WR121	57516002	1	w1279272003E	gv279272159I	w1279273651E	091107
136	WR121	57511002	1	w1279278004E	gv279278160I	w1279279652E	091107
137	WR121	57506002	1	w1279284064E	gv279284215I	w1279285657E	091107
138	WR121	57505002	1	w1279289944E	gv279290090I		091107
139	WR121	57509002	1	w1279318445E	gv279318601I	w1279320093E	091107
140	WR121	57515002	1	w1279324023E	gv279324180I	w1279325672E	091107
141	WR121	57502006	1	w1279422306E	gv279422464I	w1279423955E	091109
142	WR121	57519002	1	w1279428004E	gv279428160I	w1279429652E	091109
143	WR121	57517002	1	w1279433765E	gv279433921I	w1279435413E	091109
162	WR121	57512006	1	gv279740700I	gv279740700I	w1279742191E	091112
163	WR121	57510006	1	w1279746479E	gv279746636I	w1279748128E	091112
164	WR121	57514006	1	w1279752259E	gv279752416I	w1279753908E	091112
167	WR121	57501006	1	w1279775045E	gv279775201I	w1279776693E	091113
168	WR121	57503006	1	w1279827363E	gv279827520I	w1279829013E	091113
169	WR121	57508006	1	w1279833124E	gv279833281I	w1279834773E	091113

Table 14 : V nominal grism observations used